NEW YORK UNIVERSITY

College of Engineering
RESEARCH DIVISION
University Heights, New York 53, N. Y.

Buckling of Sandwich Cylinders under Axial Compression, Torsion, Bending, and Combined Loads

CHI-TEH WANG AND DANIEL F. DE SANTO
College of Engineering, New York University

AUGUST 1953
SPONSORED BY OFFICE OF NAVAL RESEARCH
Contract No. N6-onr-279, Task Order V

Buckling of Sandwich Cylinders Under Axial Compression, Torsion, Bending and Combined Loads*

By

Chi-Teh Wang** and Daniel F. DeSanto***

* The results reported in this paper were obtained during the course of research sponsored by Office of Naval Research under contract No. N6-onr-279, Task Order V.

** Professor of Aeronautical Engineering

*** Research Assistant

SUMMARY

During the past several years, investigation has been carried out at the Daniel Guggenheim School of Aeronautics, New York University, to study the buckling behavior of sandwich structures. The main effort has been directed towards the determination of the buckling loads of circular sandwich cylinders under different loading conditions. It was found that for cylinders with weak cores, linear theory predicts buckling loads which agree with experimental results. This is contrary to the case of homogeneous cylinders, where linear theory gives buckling loads much higher than those observed from experiments. The reason for this has been explained in Reference 11. In this report, the theory of buckling of sandwich cylinders under axial compression, torsion, and bending, and combined loads is developed in a unified manner; and the principal experimental results are presented. The interrelationship obtained between the critical loads is plotted in the form of non-dimensional interaction curves.

Symbols and Units

a	radius of cylinder to middle surface, in.
C	shear rigidity of the core; $C = (h+t)G_c$, lb. per in.
C_d	portion of boundary over which displacements are prescribed.
D	bending rigidity of a sandwich element; $D = E_f t(h+t)^2/2(1-\nu_f^2)$, lb.-in.
E	Young's modulus of elasticity, lb. per sq. in.
E_s	secant modulus of elasticity, lb. per sq. in.
F	$2tE_f/a^2$, lb. per cu. in.
G	shear modulus; $G = E/2(1+\nu)$, lb. per sq. in.
h	thickness of core layer, in.
I	moment of inertia of sandwich cylinder about its diameter, in.^{4}
J	complementary energy, in.-lb.
k_s	buckling coefficient
K_t	torsional instability coefficient
l	length of cylinder, in.
L	lC/Mat
L'	$\left[1-(N_1/C)\right] lC/Mat$
$\bar{L}$	$\left[1+n_1^2/\lambda^2-N_1/C-(T/\pi a^2 C)(n_1/\lambda)\right] lC/Mat$
$\bar{L}'$	$\left[1+n_1^2/\lambda^2-N_1/C+(T/\pi a^2 C)(n_1/\lambda)\right] lC/Mat$
L_x	longitudinal wave length, in.
L_θ	circumferential wave length, in.
L_f	free length of cylinder, in.
m	number of half waves longitudinally
M	applied bending moment, in.-lb.
M_x, M_y, M_{xy}	resultant bending and twisting moments in the composite structure, in.-lb. per in.
M_{nx}, M_{ny}	x- and y-components of the resultant moment on the boundary in.-lb. per in.
N_x, N_y	resultant normal forces in the composite structure, lb. per in.

N_{xy}	resultant shearing force in composite structure, lb. per in.
$\bar{N}_x, \bar{N}_y$	resultant median-surface normal forces, lb. per in.
$\bar{N}_{xy}$	resultant median-surface shearing force, lb. per in.
N_1	applied normal force in axial direction, lb. per in.
n	number of full waves circumferentially
p	external lateral pressure on cylinder surface lb. per sq. in.
q	$1/2(p_u - p_l)$ lb. per sq. in.
Q	left-hand side of Modified Donnell's Equation with assumed function w substituted
Q_x, Q_y	shear stress resultants in composite structure normal to middle surface, lb. per in.
Q_n	resultant Q on boundary, lb. per in.
R	radius of curvature of median surface of sandwich structure, in.
R_B	bending stress ratio, $R_B = 2Mat/IC$
R_C	compression stress ratio, $R_C = N_1/C$
R_T	torsion stress ratio, $R_T = T/2\pi a^2 C$
t	thickness of face layer, in.
T	applied torsional moment (Fig. 2), lb.-in.
u, v, w,	displacements in x-, y-, and z-directions respectively of a point in middle surface of cylinder, in.
U	work done by the force resultants due to large deflection, in.-lb.
V	strain energy, in-lb.
W	potential of external forces and moments, in.-lb.
x, y, z	rectangular coordinates (Fig. 2)
X_n, Y_n	x- and y-components of the force resultant acting on the boundary, lb. per in.
Z	curvature parameter, $Z = (1-\nu_f^2)^{1/2} l^2/2at$
α	$(h+t)^2/a^2$
β_x, β_y	components of change of slope of normal to middle surface of sandwich shell.

γ	$(h+t)G_c/E_f t$
γ'	shearing strain
δ	first variation
ε	unit elongation, in. per in.
θ	polar co-ordinate (Fig. 2)
λ	mra/λ
$\lambda_1, \lambda_2, \lambda_3, \lambda_4, \lambda_5, \lambda_6$	Lagrangian multipliers
ν	Poisson's ratio
σ	normal stress, lb. per sq. in.
τ	shear stress, lb. per sq. in.
∇^2	operator, $(\frac{\partial^2}{\partial x^2} + \frac{\partial^2}{\partial y^2}) = (\frac{\partial^2}{\partial x^2} + \frac{\partial^2}{a^2 \partial \theta^2})$
∇^4	operator, $(\frac{\partial^2}{\partial x^2} + \frac{\partial^2}{\partial y^2})^2 = (\frac{\partial^4}{\partial x^4} + 2\frac{\partial^4}{\partial x^2 \partial y^2} + \frac{\partial^4}{\partial y^4}) = (\frac{\partial^2}{\partial x^2} + \frac{\partial^2}{a^2 \partial \theta^2})^2$
∇^8	operator, $(\frac{\partial^2}{\partial x^2} + \frac{\partial^2}{\partial y^2})^4 = (\frac{\partial^2}{\partial x^2} + \frac{\partial^2}{a^2 \partial \theta^2})^4$

Subscripts

f	face layer
c	core layer
ℓ	lower face layer
u	upper face layer
m	median surface
cr	critical (buckling)

Introduction

A sandwich-type structure consists of two external layers of thin high-strength material and a thick internal layer of light-weight material. The former are usually called the face layers and the latter the core. The basic advantage of a sandwich structure is its high bending rigidity and consequently buckling strength and its relatively light weight. The use of sandwich-type structural elements for aircraft construction has received considerable amount of attention with the development of high-speed aircraft. This is because at high speed the surface of the plane must be maintained smooth without buckling during flight. This is a requirement which the ordinary thin-sheet-stringer type of construction cannot meet without undue sacrifice of the weight economy.

The buckling and bending of sandwich-type beams and flat plates have been studied by many investigators. During the past several years, investigations have been carried out at the Daniel Guggenheim School of Aeronautics of New York University to study the buckling behavior of sandwich cylinders under various loading conditions. This report summarizes the principal theoretical and experimental findings of these investigations.

Theoretical Development

Derivation of the Governing Equations

In order to derive a complete system of equations for the sandwich shell composed of face layers and core layer, it is necessary to consider separately the statics of the face layers and that of the core layer of the shell. Combination of the results obtained for the components will lead to those differential equations of equilibrium for the composite shell. The face layers are treated like thin shells of thickness t having negligible bending stiffness about their own middle surface. The loads applied to these face shells are of two kinds: external loads and loads caused by the stresses in the core layer (Fig. 1). The core layer, of thickness h, is assumed to behave like a three-dimensional elastic continuum in which those stresses which are parallel to the faces are negligible compared with the transverse shear and normal stresses.

Assuming large deflection, the equilibrium differential equations for the upper face layer are the following:

$$\frac{\partial N_{xu}}{\partial x}\left(1 + \frac{h+t}{2R}\right) + \frac{\partial N_{yxu}}{\partial y} + \frac{N_{yu}}{R}\frac{\partial w_u}{\partial x} + \tau_{xu}\left(1 + \frac{h+t}{2R}\right) = 0 \qquad (1)$$

$$\frac{\partial N_{xyu}}{\partial x}\left(1 + \frac{h+t}{2R}\right) + \frac{\partial N_{yu}}{\partial y} - \frac{N_{xyu}}{R}\frac{\partial w_u}{\partial x} + \tau_{yu}\left(1 + \frac{h+t}{2R}\right) = 0 \qquad (2)$$

$$\frac{N_{yu}}{R} + \frac{\partial}{\partial x}\left[N_{xu}\left(1 + \frac{h+t}{2R}\right)\frac{\partial w_u}{\partial x} + N_{yxu}\frac{\partial w_u}{\partial y}\right]$$

$$+ \frac{\partial}{\partial y}\left[N_{xyu}\frac{\partial w_u}{\partial x} + \frac{N_{yu}}{1 + \frac{h+t}{2R}}\frac{\partial w_u}{\partial y}\right] + p_u\left(1 + \frac{h+t}{2R}\right)$$

$$+ \sigma_{zu}\left(1 + \frac{h+t}{2R}\right) + \tau_{xu}\frac{\partial w_u}{\partial x}\left(1 + \frac{h+t}{2R}\right) + \tau_{yu}\frac{\partial w_u}{\partial y} = 0 \qquad (3)$$

Similarly, for the lower face layer, the equilibrium equations are

$$\frac{\partial N_{xl}}{\partial x}\left(1 - \frac{h+t}{2R}\right) + \frac{\partial N_{yxl}}{\partial y} + \frac{N_{yl}}{R}\frac{\partial w_l}{\partial x} - \tau_{xl}\left(1 - \frac{h+t}{2R}\right) = 0 \qquad (4)$$

$$\frac{\partial N_{xyl}}{\partial x}\left(1 - \frac{h+t}{2R}\right) + \frac{\partial N_{yl}}{\partial y} - \frac{N_{xyl}}{R}\frac{\partial w_l}{\partial x} - \tau_{yl}\left(1 - \frac{h+t}{2R}\right) = 0 \qquad (5)$$

$$\frac{N_{yl}}{R} + \frac{\partial}{\partial x}\left[N_{xl}\left(1 - \frac{h+t}{2R}\right)\frac{\partial w_l}{\partial x} + N_{yxl}\frac{\partial w_l}{\partial y}\right]$$

$$+ \frac{\partial}{\partial y}\left[N_{xyl}\frac{\partial w_l}{\partial x} + \frac{N_{yl}}{\left(1 - \frac{h+t}{2R}\right)}\frac{\partial w_l}{\partial y}\right] + p_l\left(1 - \frac{h+t}{2R}\right)$$

$$- \sigma_{zl}\left(1 - \frac{h+t}{2R}\right) - \tau_{xl}\frac{\partial w_l}{\partial x}\left(1 - \frac{h+t}{2R}\right) - \tau_{yl}\frac{\partial w_l}{\partial y} = 0 \qquad (6)$$

where the subscripts u and ℓ denote the upper and lower surfaces respectively.

Under the assumption of negligible face-parallel core stresses, the equilibrium equations for the core layer are

$$\frac{\partial}{\partial z}\left[\left(1-\frac{z}{R}\right)\tau_x\right]=0 \tag{7}$$

$$\frac{\partial}{\partial z}\left[\left(1-\frac{z}{R}\right)^2\tau_y\right]=0 \tag{8}$$

$$\frac{\partial}{\partial x}\left[\left(1-\frac{z}{R}\right)\tau_x\right]+\frac{\partial}{\partial y}\tau_y+\frac{\partial}{\partial z}\left[\left(1-\frac{z}{R}\right)\sigma_z\right]=0 \tag{9}$$

Let the values of the three stress components at the middle surface (z=0) be designated by the subscript m. Integration of Eqs. (7) to (9) results in

$$\left(1-\frac{z}{R}\right)\tau_x=\tau_{xm} \tag{10}$$

$$\left(1-\frac{z}{R}\right)^2\tau_y=\tau_{ym} \tag{11}$$

$$\left(1-\frac{z}{R}\right)\sigma_z=\sigma_{zm}-z\left[\frac{\partial\tau_y}{\partial y}+\frac{\partial}{\partial x}\left(1-\frac{z}{R}\right)\tau_x\right] \tag{12}$$

Let Q_x and Q_y be the resultant transverse shear forces. Then

$$Q_x=\int_{-\frac{h+t}{2}}^{+\frac{h+t}{2}}\tau_x\left(1-\frac{z}{R}\right)dz=(h+t)\,\tau_{xm} \tag{13}$$

$$Q_y=\int_{-\frac{h+t}{2}}^{+\frac{h+t}{2}}\tau_y\,dz=\frac{(h+t)\tau_{ym}}{1-\left(\frac{h+t}{2R}\right)^2} \tag{14}$$

From Eqs. (10), (11), (13) and (14), the following relations may be obtained:

$$\left(1 + \frac{h+t}{2R}\right) \tau_{xu} - \left(1 - \frac{h+t}{2R}\right) \tau_{xl} = 0$$

$$\left(1 + \frac{h+t}{2R}\right) \tau_{yu} - \left(1 - \frac{h+t}{2R}\right) \tau_{yl} = -\frac{Q_y}{R}$$

$$\frac{h+t}{2}\left[\left(1 + \frac{h+t}{2R}\right) \tau_{xu} + \left(1 - \frac{h+t}{2R}\right) \tau_{xl}\right] = Q_x$$

$$\frac{h+t}{2}\left[\left(1 + \frac{h+t}{2R}\right) \tau_{yu} + \left(1 - \frac{h+t}{2R}\right) \tau_{yl}\right] = Q_y \qquad (15)$$

For thin sandwich shells, $\frac{h+t}{2R} << 1$. In such cases, a combination of Eqs. (12), (13), and (14) gives

$$\left(1 + \frac{h+t}{2R}\right) \sigma_{zu} - \left(1 - \frac{h+t}{2R}\right) \sigma_{zl} = \frac{\partial Q_x}{\partial x} + \frac{\partial Q_y}{\partial y} \qquad (16)$$

In view of the fact that all face-parallel core stresses are neglected, the face-parallel stress resultants and couples of the composite shell are due to the stresses in the face layers only and may be obtained as follows:

$$N_x = N_{xu}\left(1 + \frac{h+t}{2R}\right) + N_{xl}\left(1 - \frac{h+t}{2R}\right)$$

$$N_y = N_{yu} + N_{yl}$$

$$N_{xy} = N_{xyu}\left(1 + \frac{h+t}{2R}\right) + N_{xyl}\left(1 - \frac{h+t}{2R}\right) \qquad (17)$$

$$N_{yx} = N_{yxu} + N_{yxl}$$

$$M_x = \frac{h+t}{2}\left[-N_{xu}\left(1+\frac{h+t}{2R}\right)+N_{xl}\left(1-\frac{h+t}{2R}\right)\right]$$

$$M_y = \frac{h+t}{2}\left[-N_{yu}+N_{yl}\right]$$

$$M_{xy} = \frac{h+t}{2}\left[-N_{xyu}\left(1+\frac{h+t}{2R}\right)+N_{xyl}\left(1-\frac{h+t}{2R}\right)\right]$$

$$M_{yx} = \frac{h+t}{2}\left[-N_{yxu}+N_{yxl}\right] \qquad \text{(17 cont'd.)}$$

$$p = p_u\left(1+\frac{h+t}{2R}\right)+p_l\left(1-\frac{h+t}{2R}\right)$$

$$q = \frac{1}{2}\left[p_u\left(1+\frac{h+t}{2R}\right)-p_l\left(1-\frac{h+t}{2R}\right)\right]$$

$$\sigma_{zm} = \frac{1}{2}\left[\sigma_{zu}\left(1+\frac{h+t}{2R}\right)+\sigma_{zl}\left(1-\frac{h+t}{2R}\right)\right]$$

Since $N_{yxu} = N_{xyu}$ and $N_{yxl} = N_{xyl}$ and $\frac{h+t}{2R} \ll 1$, one may write $N_{xy} = N_{yx}$ and $M_{xy} = M_{yx}$.

Define the deformation of the composite shell to be

$$w = (w_u + w_l)/2$$

and

$$e = (w_u - w_l)/(h+t) \qquad (18)$$

where w represents the effective transverse deflection of the middle surface and e represents the effective transverse normal strain for the composite shell. From these definitions, w_u and w_l may be written in terms of w and e as follows:

$$w_u = w + \frac{(h+t)e}{2} \tag{19}$$

$$w_b = w - \frac{(h+t)e}{2} \tag{20}$$

With equations (15) to (20), the following equations may be obtained by carrying out addition as well as subtraction of equations (1) and (4), and (2) and (5).

$$\frac{\partial N_x}{\partial x} + \frac{\partial N_{xy}}{\partial y} + \frac{N_y}{R}\frac{\partial w}{\partial x} - \frac{M_y}{R}\frac{\partial e}{\partial x} = 0 \tag{21}$$

$$\frac{\partial N_{xy}}{\partial x} + \frac{\partial N_y}{\partial y} - \frac{N_{xy}}{R}\frac{\partial w}{\partial x} + \frac{M_{xy}}{R}\frac{\partial e}{\partial x} - \frac{Q_y}{R} = 0 \tag{22}$$

$$\frac{\partial M_x}{\partial x} + \frac{\partial M_{xy}}{\partial y} + \frac{M_y}{R}\frac{\partial w}{\partial x} - \frac{(h+t)^2 N_y}{4R}\frac{\partial e}{\partial x} - Q_x = 0 \tag{23}$$

$$\frac{\partial M_{xy}}{\partial x} + \frac{\partial M_y}{\partial y} - \frac{M_{xy}}{R}\frac{\partial w}{\partial x} + \frac{(h+t)^2 N_{xy}}{4R}\frac{\partial e}{\partial x} - Q_y = 0 \tag{24}$$

From equations (3) and (6) may be derived the following two relations:

$$\frac{N_y}{R} + \frac{\partial}{\partial x}\left(N_x\frac{\partial w}{\partial x} + N_{xy}\frac{\partial w}{\partial y}\right) + \frac{\partial}{\partial y}\left(N_{xy}\frac{\partial w}{\partial x} + N_y\frac{\partial w}{\partial y}\right)$$

$$- \frac{\partial}{\partial x}\left(M_x\frac{\partial e}{\partial x} + M_{xy}\frac{\partial e}{\partial y}\right) - \frac{\partial}{\partial y}\left(M_{xy}\frac{\partial e}{\partial x} + M_y\frac{\partial e}{\partial y}\right) + p$$

$$+ \left(\frac{\partial Q_x}{\partial x} + \frac{\partial Q_y}{\partial y}\right) - \frac{Q_y}{R}\frac{\partial w}{\partial y} + \left(Q_x\frac{\partial e}{\partial x} + Q_y\frac{\partial e}{\partial y}\right) = 0 \tag{25}$$

$$\frac{M_y}{R} + \frac{\partial}{\partial x}\left(M_x \frac{\partial w}{\partial x} + M_{xy} \frac{\partial w}{\partial y}\right) + \frac{\partial}{\partial y}\left(M_{xy} \frac{\partial w}{\partial x} + M_y \frac{\partial w}{\partial y}\right)$$

$$- \frac{(h+t)^2}{4} \frac{\partial}{\partial x}\left(N_x \frac{\partial e}{\partial x} + N_{xy} \frac{\partial e}{\partial y}\right) - \frac{(h+t)^2}{4} \frac{\partial}{\partial y}\left(N_{xy} \frac{\partial e}{\partial x} + N_y \frac{\partial e}{\partial y}\right)$$

$$- (h+t)(f_z+q) - \left(Q_x \frac{\partial w}{\partial x} + Q_y \frac{\partial w}{\partial y}\right) + \frac{(h+t)^2}{4} \frac{Q_v}{R} = 0 \qquad (26)$$

When the radius of curvature R becomes infinite, Equations (21) to (26) reduce to the same equations obtained by Reissner [1,2]. When the effective transverse normal strain e for the composite shell is neglected, Equations (21) to (25) reduce to the usual equations of force and moment equilibrium for homogeneous shells. Eq. (26) has no counterpart in the theory of homogeneous shells, in the sense that the corresponding equation for the homogeneous shell contains information that is not of practical interest and is therefore never formulated. This equation gives the local change of thickness of the shell caused directly by the external loads by way of the non-linear terms having stress resultants and couples as factors.

In order to solve these differential equations of equilibrium, it is necessary to derive an appropriate system of stress-displacement relations. This may be done by the use of the method of complementary energy, which states that the true state of stress is distinguished from all statically correct states of stress by the condition that the complementary energy be a stationary value. In the linear elasticity theory, for a material obeying Hooke's law and for given surface stresses or displacements the complementary energy is the difference of the strain energy V and of the virtual work W which the surface stresses do over that portion of the surface where the displacements are prescribed. In the non-linear theory of elasticity it can be shown[4] that the expression for the complementary energy may be derived from the expression for the potential energy by a Legendre type of transformation, and in the case of a thin shell with finite deflection, the complementary energy J is

$$J = V + U - W \tag{27}$$

where V is the strain energy, W, the work function and U, the work done by the stress resultants in the middle plane due to large deflection, namely

$$U = \frac{1}{2}\iint\left[N_x\left(\frac{\partial w}{\partial x}\right)^2 + 2N_{xy}\frac{\partial w}{\partial x}\frac{\partial w}{\partial y} + N_y\left(\frac{\partial w}{\partial y}\right)^2\right]dx\,dy \tag{28}$$

Denote the properties of face layers and the core by the subscripts f and c respectively. The strain energy of the face layers and the core may be written as[1]

$$V_f = \frac{1}{2}\iint\left\{\frac{1}{2tE_f}\left[N_x^2 + N_y^2 - 2\nu_f N_x N_y + 2(1+\nu_f)N_{xy}^2\right]\right.$$

$$\left.\frac{2}{t(h+t)^2E_f}\left[M_x^2 + M_y^2 - 2\nu_f M_x M_y + 2(1+\nu_f)M_{xy}^2\right]\right\}dx\,dy$$

$$V_c = \frac{1}{2}\iint\left\{\frac{Q_x^2 + Q_y^2}{(h+t)C_c} + \frac{h+t}{E_c}\left[\sigma_{zm}^2 + \frac{1}{12}\left(\frac{\partial Q_x}{\partial x} + \frac{\partial Q_y}{\partial y}\right)^2\right]\right\}dx\,dy \tag{29}$$

The work done by the stress resultant due to large deflection is

$$U = \frac{1}{2}\iint\left[N_{xu}\left(\frac{\partial w_u}{\partial x}\right)^2 + 2N_{xyu}\frac{\partial w_u}{\partial x}\frac{\partial w_u}{\partial y} + N_{yu}\left(\frac{\partial w_u}{\partial y}\right)^2\right]\left(1 + \frac{h+t}{2R}\right)dx\,dy$$

$$+ \frac{1}{2}\iint\left[N_{xl}\left(\frac{\partial w_l}{\partial x}\right)^2 + 2N_{xyl}\frac{\partial w_l}{\partial x}\frac{\partial w_l}{\partial y} + N_{yl}\left(\frac{\partial w_l}{\partial y}\right)^2\right]\left(1 - \frac{h+t}{2R}\right)dx\,dy$$

With the aid of Equations (17), (19) and (20), U becomes

$$U = \frac{1}{2}\iint\left[N_x\left(\frac{\partial w}{\partial x}\right)^2 + 2N_{xy}\frac{\partial w}{\partial x}\frac{\partial w}{\partial y} + N_y\left(\frac{\partial w}{\partial y}\right)^2\right] dx\,dy$$

$$+ \frac{(h+t)^2}{8}\iint\left[N_x\left(\frac{\partial e}{\partial x}\right)^2 + 2N_{xy}\frac{\partial e}{\partial x}\frac{\partial e}{\partial y} + N_y\left(\frac{\partial e}{\partial y}\right)^2\right] dx\,dy$$

$$- \iint\left[M_x\frac{\partial e}{\partial x}\frac{\partial w}{\partial x} + M_{xy}\left(\frac{\partial e}{\partial x}\frac{\partial w}{\partial y} + \frac{\partial e}{\partial y}\frac{\partial w}{\partial x}\right)\right.$$

$$\left. + M_y\frac{\partial e}{\partial y}\frac{\partial w}{\partial y}\right] dx\,dy \qquad (30)$$

The work function W is

$$W = \oint_{C_d}\left[X_{nu}u_u + Y_{nu}v_u + \left(X_{nu}\frac{\partial w_u}{\partial x} + Y_{nu}\frac{\partial w_u}{\partial y}\right)w_u\right] ds$$

$$+ \oint_{C_d}\left[X_{nl}u_l + Y_{nl}v_l + \left(X_{nl}\frac{\partial w_l}{\partial x} + Y_{nl}\frac{\partial w_l}{\partial y}\right)w_l\right] ds$$

$$- \oint_{C_d} w\,Q_n\,ds + \oint_{C_d}\frac{h+t}{12E_c}\left(\frac{\partial Q_x}{\partial x} + \frac{\partial Q_y}{\partial y}\right)Q_n\,ds$$

where the last two integrals are the work done by the shear stress resultant in the core. The first one of these two is the work done due to the displacement of the middle surface and the second due to compression of the

core.

Define the displacements of the middle surface and the resultant load on the boundary of the composite shell to be as follows:

$$u = \frac{1}{2}(u_u + u_l); \qquad v = \frac{1}{2}(v_u + v_l);$$

$$\beta_x = \frac{1}{h+t}(-u_u + u_l); \qquad \beta_y = \frac{1}{h+t}(-v_u + v_l);$$

$$X_n = X_{nu} + X_{nl}; \qquad Y_n = Y_{nu} + Y_{nl};$$

$$M_{nx} = \frac{h+t}{2}(-X_{nu} + X_{nl}); \qquad M_{ny} = \frac{h+t}{2}(-Y_{nu} + Y_{nl})$$

The work function W becomes

$$W = \oint_{C_d} \Big[X_n u + Y_n v + \left(X_n \frac{\partial w}{\partial x} + Y_n \frac{\partial w}{\partial y} + Q_n\right) w$$

$$+ M_{nx}\beta_x + M_{ny}\beta_y - \left(M_{nx}\frac{\partial \beta_x}{\partial x} + M_{ny}\frac{\partial \beta_y}{\partial y}\right) w$$

$$- \left(M_{nx}\frac{\partial w}{\partial x} + M_{ny}\frac{\partial w}{\partial y}\right)\epsilon + \frac{(h+t)^2}{4}\left(X_n\frac{\partial \epsilon}{\partial x} + Y_n\frac{\partial \epsilon}{\partial y}\right)\epsilon$$

$$+ \frac{h+t}{12E_c}\left(\frac{\partial Q_x}{\partial y} + \frac{\partial Q_y}{\partial y}\right)Q_n \Big] ds \qquad (31)$$

Introducing the Lagrangian multipliers λ_1 to λ_6 and carrying out the first variation with respect to N_x, N_y, N_{xy}, M_x, M_y, M_{xy}, Q_x and Q_y and σ_z independently, the relation

$$\delta L = \delta V_f + \delta V_c + \delta U + \delta W$$

$$+ \delta \iint_{A_1} \left[\frac{\partial N_x}{\partial x} + \frac{\partial N_{xy}}{\partial y} + \frac{N_y}{R} \frac{\partial w}{\partial x} - \frac{M_y}{R} \frac{\partial e}{\partial x} \right]$$

$$+ \lambda_2 \left[\frac{\partial N_{xy}}{\partial x} + \frac{\partial N_y}{\partial y} - \frac{N_{xy}}{R} \frac{\partial w}{\partial x} + \frac{M_{xy}}{R} \frac{\partial e}{\partial x} - \frac{Q_y}{R} \right]$$

$$+ \lambda_3 \left[\frac{N_y}{R} + \frac{\partial}{\partial x} (N_x \frac{\partial w}{\partial x}) + \frac{\partial}{\partial y} (N_{xy} \frac{\partial w}{\partial x}) \right.$$

$$+ \frac{\partial}{\partial x} (N_{xy} \frac{\partial w}{\partial y}) + \frac{\partial}{\partial y} (N_y \frac{\partial w}{\partial y}) - \frac{\partial}{\partial x} (M_x \frac{\partial e}{\partial x}) - \frac{\partial}{\partial y} (M_{xy} \frac{\partial e}{\partial x})$$

$$- \frac{\partial}{\partial x} (M_{xy} \frac{\partial e}{\partial y}) - \frac{\partial}{\partial y} (M_y \frac{\partial e}{\partial y}) + p + (\frac{\partial Q_x}{\partial x} + \frac{\partial Q_y}{\partial y})$$

$$\left. + (Q_x \frac{\partial e}{\partial x} + Q_y \frac{\partial e}{\partial y}) - \frac{Q_y}{R} \frac{\partial w}{\partial y} \right]$$

$$+ \lambda_4 \left[\frac{\partial M_x}{\partial x} + \frac{\partial M_{xy}}{\partial y} + \frac{M_y}{R} \frac{\partial w}{\partial x} - \frac{(h+t)^2}{4} \frac{N_y}{R} \frac{\partial e}{\partial x} - Q_x \right]$$

$$+ \lambda_5 \left[\frac{\partial M_{xy}}{\partial x} + \frac{\partial M_y}{\partial y} - \frac{M_{xy}}{R} \frac{\partial w}{\partial x} + \frac{(h+t)^2}{4} \frac{N_{xy}}{R} \frac{\partial e}{\partial x} - Q_y \right]$$

$$+ \lambda_6 \left[\frac{M_y}{R} + \frac{\partial}{\partial x} (M_x \frac{\partial w}{\partial x} + M_{xy} \frac{\partial w}{\partial y}) + \frac{\partial}{\partial y} (M_{xy} \frac{\partial w}{\partial x} + M_y \frac{\partial w}{\partial y}) \right.$$

$$- \frac{(h+t)^2}{4} \frac{\partial}{\partial x}\left(N_x \frac{\partial e}{\partial x} + N_{xy} \frac{\partial e}{\partial y}\right) - \frac{(h+t)^2}{4} \frac{\partial}{\partial y}\left(N_{xy} \frac{\partial e}{\partial y} + N_y \frac{\partial e}{\partial y}\right)$$

$$- (h+t)(\sigma_z + q) - \left(Q_x \frac{\partial w}{\partial x} + Q_y \frac{\partial w}{\partial y}\right) + \frac{(h+t)^2}{4} \frac{Q_y}{R}\Bigg]\Bigg\} dx\, dy = 0 \qquad (32)$$

leads to the conditions

$$\lambda_1 = u \qquad \lambda_2 = v \qquad \lambda_3 = w$$
$$\lambda_4 = \beta_x \qquad \lambda_5 = \beta_y \qquad \lambda_6 = e \qquad (33)$$

on the boundary. As equation (32) also holds for any part of the structure if the boundary displacements referring to this part are identified with the displacement occurring in the actual solution of the problem, it follows that the Lagrange's multipliers throughout the structure are related to the generalized displacements in the interior of the boundary. It follows that equation (33) also holds true now in the interior.

Using equations (33), the Euler equations of $\delta L = 0$ in the Calculus of Variations give the following stress-displacement relations:

$$\frac{N_x - \nu_f N_y}{2tE_f} = \frac{\partial u}{\partial x} + \frac{1}{2}\left[\left(\frac{\partial w}{\partial x}\right)^2 + \frac{(h+t)^2}{4}\left(\frac{\partial e}{\partial x}\right)^2\right]$$

$$\frac{N_y - \nu_f N_x}{2tE_f} = \frac{\partial v}{\partial y} - \frac{w}{R} + \frac{1}{2}\left[\left(\frac{\partial w}{\partial y}\right)^2 + \frac{(h+t)^2}{4}\left(\frac{\partial e}{\partial y}\right)^2\right] - \frac{u}{R}\frac{\partial w}{\partial x}$$

$$+ \frac{(h+t)^2}{4} \frac{\beta_x}{R} \frac{\partial e}{\partial x}$$

$$\frac{2(1+\nu_f)N_{xy}}{2tE} = \frac{\partial u}{\partial y} + \frac{\partial v}{\partial x} + \frac{\partial w}{\partial x}\frac{\partial w}{\partial y} + \frac{(h+t)^2}{4}\frac{\partial e}{\partial x}\frac{\partial e}{\partial y}$$

$$+ \frac{v}{R}\frac{\partial w}{\partial x} - \frac{(h+t)^2}{4}\frac{\beta_y}{R}\frac{\partial e}{\partial x}$$

$$\frac{M_x - \nu_f M_y}{t(h+t)^2 E_f/2} = \frac{\partial \beta_x}{\partial x} + \frac{\partial w}{\partial x}\frac{\partial e}{\partial x}$$

$$\frac{M_y - \nu_f M_x}{t(h+t)^2 E_f/2} = \frac{\partial \beta_y}{\partial y} + \frac{\partial w}{\partial y}\frac{\partial e}{\partial y} + \frac{u}{R}\frac{\partial e}{\partial x} - \frac{\beta_x}{R}\frac{\partial w}{\partial x} + \frac{e}{R}$$

$$\frac{4(1+\nu_f)M_{xy}}{t(h+t)^2 E_f} = \frac{\partial \beta_x}{\partial y} + \frac{\partial \beta_y}{\partial x} - \frac{\partial w}{\partial x}\frac{\partial e}{\partial y} - \frac{\partial w}{\partial y}\frac{\partial e}{\partial x} - \frac{v}{R}\frac{\partial e}{\partial x} + \frac{\beta_y}{R}\frac{\partial w}{\partial x}$$

$$\frac{Q_x}{(h+t)G_c} - \frac{(h+t)}{12E_c}\frac{\partial}{\partial x}\left(\frac{\partial Q_x}{\partial x} + \frac{\partial Q_y}{\partial y}\right) = \beta_x + \frac{\partial w}{\partial x} - \frac{\partial e}{\partial x}w - \frac{\partial w}{\partial x}e$$

$$\frac{Q_y}{(h+t)G_c} - \frac{h+t}{12E_c}\frac{\partial}{\partial y}\left(\frac{\partial Q_x}{\partial x} + \frac{\partial Q_y}{\partial y}\right) = \beta_y + \frac{\partial w}{\partial y} - \frac{\partial e}{\partial y}w - e\frac{\partial w}{\partial y}$$

$$+ \frac{v}{R} + \frac{w}{R}\frac{\partial w}{\partial y} + \frac{(h+t)^2}{4}\frac{e}{R}$$

$$e = -\sigma_{zm}/E_c \qquad (34)$$

In the case of flat sandwich plates, $R \to \infty$, the stress-strain relations (34) reduce to exactly those obtained by Reissner [2,3]. In the case of homogeneous shells ($G_c = \frac{1}{2}E_c \to \infty$, $e \to 0$), equations (34) then

reduce to the stress-strain relations for homogeneous shells when finite deflection is assumed.

If buckling of the sandwich structure as a unit is to be studied, the effect of the transverse normal stress deformability can usually be neglected and therefore one may assume $E_c = \infty$ and $e = 0$. In the buckling theory, the displacements u, v, and w are the displacements occurring during buckling and the quantities N_x, N_y, etc. represent only the changes in the internal forces during buckling. If we denote the median surface stresses by $\bar{N}_x$, $\bar{N}_y$, and $\bar{N}_{xy}$ and neglect the terms which Donnell [5] justified as being small, the equilibrium equations become

$$\frac{\partial N_x}{\partial x} + \frac{\partial N_{xy}}{\partial y} = 0 \tag{35}$$

$$\frac{\partial N_{xy}}{\partial x} + \frac{\partial N_y}{\partial y} = 0 \tag{36}$$

$$\frac{\partial Q_x}{\partial x} + \frac{\partial Q_y}{\partial y} - \frac{\bar{N}_y + N_y}{R} + \bar{N}_x \frac{\partial^2 w}{\partial x^2} + \bar{N}_y \frac{\partial^2 w}{\partial y^2} + 2\bar{N}_{xy} \frac{\partial^2 w}{\partial x \partial y} = 0 \tag{37}$$

$$\frac{\partial M_x}{\partial x} + \frac{\partial M_{xy}}{\partial y} - Q_x = 0 \tag{38}$$

$$\frac{\partial M_{xy}}{\partial x} + \frac{\partial M_y}{\partial y} - Q_y = 0 \tag{39}$$

and the stress-displacement relations become

$$\frac{N_x - \nu_f N_y}{2tE_f} = \frac{\partial u}{\partial x}$$

$$\frac{N_y - \nu_f N_x}{2tE_f} = \frac{1}{R}\frac{\partial v}{\partial \theta} - \frac{w}{R} \tag{40}$$

$$\frac{2(1+\nu_f)N_{xy}}{2tE_f} = \frac{1}{R}\frac{\partial u}{\partial \theta} + \frac{\partial v}{\partial x}$$

$$\frac{M_x - \nu_f M_y}{t(h+t)^2 E_f/2} = \frac{\partial \beta_x}{\partial x} \qquad \text{(40 cont'd.)}$$

$$\frac{M_y - \nu_f M_x}{t(h+t)^2 E_f/2} = \frac{1}{R}\frac{\partial \beta_y}{\partial \theta}$$

$$\frac{4(1+\nu_f)M_{xy}}{t(h+t)^2 E_f} = \frac{\partial \beta_x}{\partial y} + \frac{1}{R}\frac{\partial \beta_y}{\partial \theta}$$

$$\frac{Q_x}{(h+t)G_c} = \beta_x + \frac{\partial w}{\partial x}$$

$$\frac{Q_y}{(h+t)G_c} = \beta_y + \frac{1}{R}\frac{\partial w}{\partial \theta}$$

Equation (40) may be rewritten in the following form:

$$N_x = \frac{2tE_f}{1-\nu_f^2}\left[\frac{\partial u}{\partial x} + \nu_f\left(\frac{1}{R}\frac{\partial v}{\partial \theta} - \frac{w}{R}\right)\right]$$

$$N_y = \frac{2tE_f}{1-\nu_f^2}\left[\nu_f\frac{\partial u}{\partial x} + \frac{1}{R}\frac{\partial v}{\partial \theta} - \frac{w}{R}\right]$$

$$N_{xy} = \frac{2tE_f}{2(1+\nu_f)}\left(\frac{1}{R}\frac{\partial u}{\partial \theta} + \frac{\partial v}{\partial x}\right) \qquad (41)$$

$$M_x = \frac{(h+t)^2 tE_f}{2(1-\nu_f^2)}\left(\frac{\partial \beta_x}{\partial x} + \nu_f\frac{1}{R}\frac{\partial \beta_y}{\partial \theta}\right)$$

$$M_y = \frac{(h+t)^2 t E_f}{2(1-\nu_f^2)} \left(\nu_f \frac{\partial \beta_x}{\partial x} + \frac{1}{R} \frac{\partial \beta_y}{\partial \theta}\right)$$

$$M_{xy} = \frac{(h+t)^2 t E_f}{2(1+\nu_f)} \left(\frac{1}{R} \frac{\partial \beta_x}{\partial \theta} + \frac{\partial \beta_y}{\partial x}\right)$$

(41 cont'd.)

$$Q_x = (h+t)\, G_c \left(\beta_x + \frac{\partial w}{\partial x}\right)$$

$$Q_y = (h+t)\, G_c \left(\beta_y + \frac{1}{R} \frac{\partial w}{\partial \theta}\right)$$

Substituting these relations into equations (35) through (39) and eliminating u, v, β_x, and β_y, one obtains finally

$$D \nabla^8 w + \left(1 - \frac{D}{C} \nabla^2\right) \left[\frac{2tE_f}{R^2} \frac{\partial^4 w}{\partial x^4} - \nabla^4 \left(\bar{N}_x \frac{\partial^2 w}{\partial x^2} + 2\bar{N}_{xy} \frac{\partial^2 w}{\partial x \partial y} + \bar{N}_y \frac{\partial^2 w}{\partial y^2}\right)\right] = 0 \qquad (42)$$

where $\nabla^2 = \partial^2/\partial x^2 + \partial^2/\partial y^2$, $D = E_f t(h+t)^2/2(1-\nu_f^2)$

and $C = (h+t)\, G_c$.

Equation (42) is the Modified Donnell's Equation for curved sandwich plates and sandwich shells and is the one which was obtained by Stein and Mayers[6] for an isotropic sandwich element.

Galerkin's Method of Approximate Solutions

We shall now proceed to solve equation (42) in the case of buckling of sandwich circular cylinders under various loadings. Let us consider the cylinder to be under the general combined loading of axial compression, torsion and bending (Fig. 2). In such a case, we have

$$\bar{N}_x = - N_1 + (2Mat/I) \cos \theta,$$

$$\bar{N}_{xy} = T/2\pi a^2, \; N_y = 0 \tag{43}$$

where N_1 is the force per unit length due to axial compression, M is the bending moment, I is the moment of inertia of the cylinder, T is the torsional moment, and a the radius of the circular section. With such a loading, equation (42) thus becomes

$$D \nabla^8 w + \left(1 - \frac{D}{C} \nabla^2\right) \left\{ \frac{2tE_f}{a^2} \frac{\partial^4 w}{\partial x^4} - \nabla^4 \left[\left(- N_1 + \frac{2Mat}{I} \cos \theta \right) \frac{\partial^2 w}{\partial x^2} + \frac{T}{\pi a^3} \frac{\partial^2 w}{\partial x \partial \theta} \right] \right\} = 0 \tag{44}$$

where y is taken as $a\theta$.

Equation (44) may be solved by means of Galerkin's method as follows: we first assume the deflection w of the cylinder after buckling in the form of a series that satisfies the boundary conditions but with undetermined parameters. For long cylinders, however, the boundary conditions at the two ends become unimportant and we may assume the deflection series without any regard for the end conditions. For a cylinder under combined axial compression and bending, w may be assumed in the following form[7],

$$w = \sin \frac{m\pi x}{\lambda} \sum_{n=0}^{\infty} A_n \cos n\theta \tag{45}$$

and for a cylinder under torsion only, the deflection after buckling is of the following form[8],

$$\begin{aligned} w &= \sum_{n=1}^{\infty} B_n \sin \left(\frac{m\pi x}{\lambda} - n\theta \right) \\ &= \sum_{n=1}^{\infty} B_n \left(\sin \frac{m\pi x}{\lambda} \cos n\theta - \cos \frac{m\pi x}{\lambda} \sin n\theta \right) \end{aligned} \tag{46}$$

Guided by these expressions, we shall assume the deflection of the cylinder in the case of combined loading as follows:

$$w = \sin\frac{m\pi x}{l}\sum_{n=0}^{n_1} A_n \cos n\theta + \cos\frac{m\pi x}{l}\sum_{n=1}^{n_1} B_n \sin n\theta. \tag{47}$$

With w expressed in a proper series, we shall next substitute this series into (44). If the expression (47) happens to be the exact solution of equation (44), after substitution equation (44) will be identically equal to zero. In general, this will not be so and the resulting expression will be a function of x and θ which we shall denote by Q. Galerkin's equations for the determination of the coefficients A_n and B_n are

$$\int_0^{2\pi}\int_0^{l} Q \sin\frac{m\pi x}{l} \cos n\theta \, a\,d\theta\,dx = 0 \tag{48}$$

$$\int_0^{2\pi}\int_0^{l} Q \cos\frac{m\pi x}{l} \sin n\theta \, a\,d\theta\,dx = 0 \tag{49}$$

which, when written out, becomes

$$\int_0^{2\pi}\int_0^{l}\left(D\nabla^8 w + F\frac{\partial^4 w}{\partial x^4} - \frac{DF}{C}\nabla^2\frac{\partial^4 w}{\partial x^4}\right)\sin\frac{m\pi x}{l}\cos n\theta\, a\,d\theta\,dx$$

$$+N_1\int_0^{2\pi}\int_0^{l}\left(\nabla^4\frac{\partial^2 w}{\partial x^2} - \frac{D}{C}\nabla^6\frac{\partial^2 w}{\partial x^2}\right)\sin\frac{m\pi x}{l}\cos n\theta\, a\,d\theta\,dx \tag{50}$$

$$-\frac{2Mat}{I}\int_0^{2\pi}\int_0^{\ell}\left(\nabla^4\frac{\partial^2 w}{\partial x^2}-\frac{D}{C}\nabla^6\frac{\partial^2 w}{\partial x^2}\right)\sin\frac{m\pi x}{\ell}\cos n\theta\cos\theta\,a\,d\theta\,dx$$

(50 cont'd.)

$$-\frac{T}{\pi a^3}\int_0^{2\pi}\int_0^{\ell}\left(\nabla^4\frac{\partial^2 w}{\partial x\partial\theta}-\frac{D}{C}\nabla^6\frac{\partial^2 w}{\partial x\partial\theta}\right)\sin\frac{m\pi x}{\ell}\cos n\theta\,a\,d\theta\,dx=0,$$

in which $F = 2tE_f/a^2$, and

$$\int_0^{2\pi}\int_0^{\ell}\left(D\nabla^8 w+F\frac{\partial^4 w}{\partial x^4}-\frac{DF}{C}\nabla^2\frac{\partial^4 w}{\partial x^4}\right)\cos\frac{m\pi x}{\ell}\sin n\theta\,a\,d\theta\,dx$$

$$+N_1\int_0^{2\pi}\int_0^{\ell}\left(\nabla^4\frac{\partial^2 w}{\partial x^2}-\frac{D}{C}\nabla^6\frac{\partial^2 w}{\partial x^2}\right)\cos\frac{m\pi x}{\ell}\sin n\theta\,a\,d\theta\,dx$$

$$-\frac{2Mat}{I}\int_0^{2\pi}\int_0^{\ell}\left(\nabla^4\frac{\partial^2 w}{\partial x^2}-\frac{D}{C}\nabla^6\frac{\partial^2 w}{\partial x^2}\right)\cos\frac{m\pi x}{\ell}\sin n\theta\cos\theta\,a\,d\theta\,dx$$

$$-\frac{T}{\pi a^3}\int_0^{2\pi}\int_0^{\ell}\left(\nabla^4\frac{\partial^2 w}{\partial x\partial\theta}-\frac{D}{C}\nabla^6\frac{\partial^2 w}{\partial x\partial\theta}\right)\cos\frac{m\pi x}{\ell}\sin n\theta\,a\,d\theta\,dx=0$$

(51)

Substituting the assumed function w into these equations and carrying out the integration, we obtain

$$\left[\frac{D(\lambda^2+n^2)^4}{a^8}+\frac{F\lambda^4}{a^4}+\frac{DF\,\lambda^4(\lambda^2+n^2)}{Ca^6}-\frac{N_1\,\lambda^2(\lambda^2+n^2)^2}{a^6}-\frac{N_1 D\,\lambda^2(\lambda^2+n^2)^3}{Ca^8}\right]A_n$$

$$+\left[\frac{Tn\,\lambda(\lambda^2+n^2)^2}{\pi a^8}+\frac{TDn\,\lambda(\lambda^2+n^2)^3}{\pi Ca^{10}}\right]B_n$$

$$+\left[\frac{Mat\,\lambda^2(\lambda^2+n^2)^2}{Ia^6}+\frac{MatD\,\lambda^2(\lambda^2+n^2)^3}{ICa^8}\right](A_{n-1}+A_{n+1})=0, \tag{52}$$

and

$$\left[\frac{D(\lambda^2+n^2)^4}{a^8}+\frac{F\lambda^4}{a^4}+\frac{DF\,\lambda^4(\lambda^2+n^2)}{Ca^6}-\frac{N_1\,\lambda^2(\lambda^2+n^2)^2}{a^6}-\frac{N_1 D\,\lambda^2(\lambda^2+n^2)^3}{Ca^8}\right]B_n$$

$$+\left[\frac{Tn\,\lambda(\lambda^2+n^2)^2}{\pi a^8}+\frac{TDn\,\lambda(\lambda^2+n^2)^3}{\pi Ca^{10}}\right]A_n \tag{53}$$

$$+\left[\frac{Mat\,\lambda^2(\lambda^2+n^2)^2}{Ia^6}+\frac{MatD\,\lambda^2(\lambda^2+n^2)^3}{ICa^8}\right](B_{n-1}+B_{n+1})=0.$$

Instead of working with these two equations, it is found convenient to combine them into the following ones. Thus, by subtracting equation (53) from (52), we obtain

$$\left[\frac{D(\lambda^2+n^2)^4}{a^8}+\frac{F\lambda^4}{a^4}+\frac{DF\lambda^4(\lambda^2+n^2)}{Ca^6}\right.$$

$$-\frac{N_1\lambda^2(\lambda^2+n^2)^2}{a^6}-\frac{N_1D\lambda^2(\lambda^2+n^2)^3}{Ca^8}$$

$$\left.-\frac{Tn\lambda(\lambda^2+n^2)^2}{\pi a^8}-\frac{TDn\lambda(\lambda^2+n^2)^3}{\pi Ca^{10}}\right]K_n$$

$$+\left[\frac{Mat\lambda^2(\lambda^2+n^2)^2}{Ia^6}+\frac{MatD\lambda^2(\lambda^2+n^2)^3}{ICa^8}\right](K_{n-1}+K_{n+1})=0, \qquad (54)$$

in which $\lambda = m\pi a/b$, $K_n = A_n - B_n$, and in which $2K_0$ is to be substituted for K_0 at $n = 1$; $K_n = 0$ when $n > n_1$. When equations (52) and (53) are added, we have

$$\left[\frac{D(\lambda^2+n^2)^4}{a^8}+\frac{F\lambda^4}{a^4}+\frac{DF\lambda^4(\lambda^2+n^2)}{Ca^6}\right.$$

$$-\frac{N_1\lambda^2(\lambda^2+n^2)^2}{a^6}-\frac{N_1D\lambda^2(\lambda^2+n^2)^3}{Ca^8}$$

$$\left.+\frac{Tn\lambda(\lambda^2+n^2)^2}{\pi a^8}+\frac{TDn\lambda(\lambda^2+n^2)^3}{\pi Ca^{10}}\right]K'_n$$

$$+\left[\frac{Mat\lambda^2(\lambda^2+n^2)^2}{Ia^6}+\frac{MatD\lambda^2(\lambda^2+n^2)^3}{ICa^8}\right](K'_{n-1}+K'_{n+1})=0, \qquad (55)$$

in which $K'_n = A_n + B_n$. Again at $n = 1$, $2K'_0$ is to be substituted for K'_0 and $K'_n = 0$ when $n > n_1$.

The substitution of n from 0 to n_1 in equations (54) and (55) results in $2n_1 + 1$ simultaneous algebraic equations for $2n_1 + 1$ unknowns. One solution to these equations is, of course, the trivial one, namely,

$$K_n = K'_n = C \quad (n = 0, 1, 2, 3, \ldots, n_1).$$

The non-trivial solution is carried out in the following section.

Determination of the Buckling Loads

Case 1. Buckling under axial compression.

If the sandwich cylinder is under the action of axial compression only, then M = T = 0 in Eqs. (54) and (55) and we obtain

$$\left[\frac{D(\lambda^2+n^2)^4}{a^8} + \frac{F\lambda^4}{a^4} + \frac{DF\lambda^4(\lambda^2+n^2)}{Ca^6} - \frac{N_1\lambda^2(\lambda^2+n^2)^2}{a^6} - \frac{N_1 D\lambda^2(\lambda^2+n^2)^3}{Ca^8} \right] K_n = 0 \qquad (56)$$

To find the non-trivial solutions of the above equation, we must set the coefficient of K_n equal to zero, which gives, after some simplification,

$$\frac{N_1}{C} = \frac{\gamma a(1+\frac{n^2}{\lambda^2})^4 + 4\gamma(1-\nu_f^2)\frac{1}{\lambda^4} + 2a\frac{1}{\lambda^2}(1+\frac{n^2}{\lambda^2})}{2\gamma^2(1-\nu_f^2)\frac{1}{\lambda^2}(1+\frac{n^2}{\lambda^2})^2 + \gamma a(1+\frac{n^2}{\lambda^2})^3} \qquad (57)$$

where $\gamma = (h+t)G_c/E_f t$, $a = (h+t)^2/a^2$.

In view of the presence of the sandwich cylinder parameters γ and a in equation (57), the determination of a minimum N_1 with respect to the parameters λ and n proves to be intractable analytically. Consequently, a numerical treatment was attempted. In the numerical analysis three cases were treated: (a) the core considered extremely weak in shear with $a = 10^{-4}$ and $\gamma = 2.7 \times 10^{-3}$; (b) the core considered moderately weak in shear with $a = 10^{-4}$ and $\gamma = 2.7 \times 10^{-2}$; and (c) the core considered relatively strong in shear with $a = 10^{-4}$ and $\gamma = 2.7 \times 10^{-1}$.

The values in case (a) were chosen so as to coincide with the nominal properties of the cylinders used in the experimental study. The other values were chosen as convenient multiples of the first set. The results of the numerical analysis are shown in Figs. 3,4, and 5. The values of n and λ obtained from these figures for a minimum N_1/C are given in

Table 1.

Table 1

α	γ	$\sqrt{\alpha}/\gamma$	N_1/C_{min}	n	λ
10^{-4}	2.7×10^{-3}	3.7	1.00	0	∞
10^{-4}	2.7×10^{-2}	0.37	0.626	0	18
10^{-4}	2.7×10^{-1}	0.037	0.0769	7	7

In Figs. 3 to 5, curves for only a few values of n are shown which are sufficient to ensure a minimum value of N_1/C for the corresponding λ. It was possible to make approximate analytical calculations that served as a guide to bracket the minimum n for a particular λ. This reduced the amount of calculation to the point where it was only necessary to calculate from Eq. (57), the n curve for a corresponding λ range. With this procedure, the values of N_1/C_{min} are reasonably certain, although n and λ may be in slight error.

These numerical calculations indicated that the minimum values of N_1 occurred at $n \cong 0$ and $\lambda >> 1$. By taking n = 0 in (57), we have

$$\frac{N_1}{C} = \frac{\gamma\alpha\lambda^4 + 2\alpha\lambda^2 + 4\gamma(1-\nu_f^2)}{\gamma\alpha\lambda^4 + 2\gamma^2(1-\nu_f^2)\lambda^2} \tag{58}$$

Since minimum N_1 occurs at large value of λ, we can determine the minimum N_1 from the condition

$$\partial N_1/\partial \lambda^2 = 0 \tag{59}$$

Equation (59) has the following real solutions:

$$\lambda^2 = \infty \tag{60}$$

and

$$\lambda^2 = \frac{2}{\sqrt{\alpha}} \frac{\frac{\sqrt{\alpha}}{\gamma} \pm \sqrt{1-\nu_f^2}}{1 - \frac{\alpha}{\gamma^2(1-\nu_f^2)}} \tag{61}$$

Note that from eq. (61) when

$$\frac{\sqrt{\alpha}}{\gamma} = \frac{E_f t}{G_c a} > \sqrt{1-\nu_f^2} \tag{62}$$

the only real root is $\lambda^2 = \infty$.

The normal stress in the faces at buckling is

$$\sigma_{cr} = N_1/2t$$

Substituting Eqs. (61) into Eq. (58) and simplifying, we obtain

$$\sigma_{cr} = k_s E_f \left[(h+t)/a \right] \tag{63}$$

where the buckling coefficient k_s is

$$k_s = \frac{\frac{\lambda^2(h+t)}{4(1-\nu_f^2)a} + \frac{a}{\lambda^2(h+t)} + \frac{E_f t}{2(1-\nu_f^2)G_c a}}{\frac{E_f t}{2(1-\nu_f^2)G_c a}\,\lambda^2\,\frac{(h+t)}{a}} \tag{64}$$

Values for the buckling coefficient k_s and half wave length have been computed from Eqs. (64) and (61), respectively, by taking $\nu_f = 0.3$. These data are shown in Figs. 6 and 7. When $E_f t/G_c a \geq 0.95$, the value of the buckling coefficient is

$$k_s = (1/2)\ (G_c a/E_f t) \tag{65}$$

Under these conditions, the buckling stress

$$\sigma_{cr} = (h+t)G_c/2t \tag{66}$$

has a value that is independent of the wave length.

An interesting feature of the theories illustrated in Fig. 6 is the fact there are apparently three ranges into which the shear effects of the core can be divided: (a) When $E_f t/G_c a \geq 0.95$, the core is extremely

weak in shear and $N_{cr} = (h+t)G_c$. (b) When $0.1 < E_f t/G_c a < 0.95$, the core is moderatley weak in shear and σ_{cr} is given by Eq. (60). (c) When $E_f t/G_c a < 0.1$, the core is relatively strong in shear, and the sandwich cylinder behaves essentially in the same manner as the homogeneous cylinder. While shear effects are negligible in this region, the nonlinear theory, which is necessary to describe buckling of a homogeneous cylinder, will also be required for the sandwich cylinder. The linearized solution for the buckling stress of the latter can be obtained as

$$\sigma = (1/\sqrt{1-\nu^2})E(h+t)/a$$

The strain energy solution obtained by Leggett and Hopkins[10] also agrees with the results shown in Fig. 6 when their solution is simplified for a core that does not carry any axial load. A slight difficulty in their solution which was not noted by Leggett and Hopkins is that, in the region A-A' shown in Fig. 6, the buckling stress given by their equation goes to zero, for in this region λ becomes imaginary for this branch and, consequently, the $\lambda = \infty$ branch must be used.

Case 2. Buckling under torsion

If the cylinder is under the action of torsional loads only, then $N_1 = M = 0$ in Eqs. (54) and (55) and we obtain

$$\left[\frac{D(\lambda^2+n^2)^4}{a^8} + \frac{F\lambda^4}{a^4} + \frac{DF\lambda^4(\lambda^2+n^2)}{Ca^6} \pm \frac{Tn\lambda(\lambda^2+n^2)^2}{\pi a^8} \pm \frac{TDn\lambda(\lambda^2+n^2)^3}{\pi C a^{10}} \right] K_n = 0 \qquad (67)$$

To find the non-trivial solutions, we set the coefficient of K_n equal to zero and obtain

$$\frac{T}{2\pi a^2 C} = \pm \frac{\alpha\gamma\lambda^4(1+\frac{n^2}{\lambda^2})^2 + \frac{1}{4}(1-\nu_f^2)\gamma + 2\alpha\lambda^2(1+\frac{n^2}{\lambda^2})}{4(1-\nu_f^2)\gamma^2\lambda^2\frac{n}{\lambda}(1+\frac{n^2}{\lambda^2})^2 + 2\alpha\gamma\lambda^4\frac{n}{\lambda}(1+\frac{n^2}{\lambda^2})^3} \qquad (68)$$

where the plus and minus signs indicate that the direction of T is immaterial to the buckling.

In order to find the lowest possible value of T, we may minimize the right-hand side of (68) with respect to the variables λ and (n/λ). It may be pointed out that λ and (n/λ) actually should take on only discrete values on account of the integral character of the n and m ($\lambda = m\pi/b$). However, in the case of sandwich cylinders with weak cores, it will be shown subsequently that the minimum values of T occur at very large values of λ. It is therefore possible to consider both λ and (n/λ) as continuous variables in the minimizing process.

Let us first examine the condition $\partial T/\partial\lambda = 0$. We find from this condition that either $\lambda = \infty$ or

$$\lambda^2 = \frac{2(1-\nu_f^2)\gamma}{\sqrt{\alpha}\left(1+\frac{n^2}{\lambda^2}\right)} \quad \frac{\sqrt{\alpha} \pm \sqrt{1-\nu_f^2}\ \gamma\left(1+\frac{n^2}{\lambda^2}\right)}{(1-\nu_f^2)\gamma^2\left(1+\frac{n^2}{\lambda^2}\right)^2 - \alpha} \tag{69}$$

It is evident that when

$$\frac{\sqrt{\alpha}}{\gamma} = \frac{E_f t}{G_c a} > \sqrt{1-\nu_f^2}\quad\left(1+\frac{n^2}{\lambda^2}\right) \tag{70}$$

the only real root is $\lambda^2 = \infty$.

The condition (70) corresponds to the case where the sandwich has a core weak in shear. By substituting $\lambda^2 = \infty$ in equation (68) and minimizing T with respect to (n/λ), we find

$$\frac{n}{\lambda} = + 1 \tag{71}$$

which gives

$$\left(\frac{T}{2\pi a^2 C}\right)_{cr} = \frac{N_{cr}}{C} = \pm 1 \tag{72}$$

This result for a core very weak in shear corresponds to that obtained for a sandwich cylinder under axial compression, a sandwich plate under compression, or a column. The critical loading in all these cases depends solely upon the shear rigidity of the core.

For sandwich cylinders with cores not weak in shear, it is necessary to proceed directly with the minimization of the Eq. (68) with respect to λ and the ratio (n/λ). This results in a pair of non-linear equations in λ and (n/λ) and their solutions become very tedious. Inasmuch as it is known that the linear theory does not predict adequately the buckling loads for a homogeneous cylinder, it is expected that the linear theory, on which the present analysis is based, also will not predict the buckling loads for sandwich cylinders with cores strong in shear. The reason why linear theory checks well with the experimental results in the case of sandwich cylinders with weak core has been presented in Reference 11.

Case 3. Buckling under bending

If the cylinder is under the action of bending loads only, we let $N_1=T=0$ in Eqs. (54) and (55) and we obtain

$$\left[\frac{D(\lambda^2+n^2)^4}{a^8}+\frac{F\lambda^4}{a^4}+\frac{DF\lambda^4(\lambda^2+n^2)}{Ca^6}\right]K_n$$

$$+\left[\frac{Mat\lambda^2(\lambda^2+n^2)^2}{Ia^6}+\frac{MatD\lambda^2(\lambda^2+n^2)^3}{ICa^8}\right](K_{n-1}+K_{n+1})=0 \qquad (73)$$

for $n \neq 1$ where $K_{-1}=0$. For $n=1$, $2K_0$ is to be substituted for K_0 and for $n > n_1$, $K_n=0$. For any value of n_1 taken we then have (n_1+1) equations with (n_1+1) unknowns. To obtain the non-trivial solution, we shall set the determinant of the coefficients of $K_0, K_1, K_2, \ldots, K_{n_1}$ equal to zero, from which the buckling load can be calculated. This procedure, however, requires very tedious calculation for a general sandwich cylinder.

To simplify the calculations, let us study the effect of λ on the buckling load of a sandwich cylinder with weak core. This is done by calculating the buckling load of such a cylinder with $n_1 = 1,2,3,4,5$. The results are plotted in Fig. 8. It is evident from these curves that for all those values of n_1, minimum M occurs at $\lambda \to \infty$. The convergence of ID/2Mat as n_1 increases can easily be seen from the figure.

By assuming that λ is a large number, many terms in eq. (73) can be neglected and we obtain

$$K_{n-1} + L K_n + K_{n+1} = 0 \tag{74}$$

for $n \neq 1$. $L = CI/1at$ in the above equation. For $n = 0$, we have

$$LK_0 + K_1 = 0 \tag{75}$$

and, for $n = 1$, we have

$$2K_0 + LK_1 + K_2 = 0 \tag{76}$$

To calculate the buckling load, instead of solving the determinant equation for a large number of terms, an alternative solution can be obtained as follows. We observe that Eq. (74) is a finite difference equation in terms of K_n. The trivial solution of Eqs. (74), (75) and (76) is

$$K_n = 0 \qquad (n = 0,1,2,3, \ldots)$$

The nontrivial solution of Eq. (74) is

$$K_n = A\alpha^n + B\alpha^{-n} \qquad (n = 1,2,3, \ldots) \tag{77}$$

where A and B are arbitrary constants and α is related to L by the formula

$$\alpha^2 + \alpha L + 1 = 0 \tag{78}$$

or

$$L = -(\alpha + \alpha^{-1}) \tag{79}$$

Substituting Eq. (77) into Eq. (76) and using relation (79), we find

$$2K_0 = - LK_1 - K_2 = - L\,(A\alpha + B\alpha^{-1}) - (A\alpha^2 + B\alpha^{-2})$$

$$= -A\,(\alpha^2 + \alpha L) - B(\alpha^{-2} + \alpha^{-1}L)$$

$$= A + B \qquad (80)$$

Now, equation (75) is the only one yet to be satisfied. Substituting K_0 given by Eq. (80) and K_1 given by Eq. (77) into Eq. (75) and using relation (79), we obtain

$$(A - B)\,(\alpha - \alpha^{-1}) = 0$$

for which we find $\alpha^2 = 1$ and $\alpha = \pm 1$. Hence, $L = \pm 2$ or

$$2Mat/I = \pm C = \pm (h+t)G_c \qquad (81)$$

We note that, when $\alpha = \pm 1$, the two roots of Eq. (78) are equal and Eq. (77) must assume the form

$$K_n = (A + nB)\alpha^n$$

But K_n must be finite when $n \to \infty$; we have, therefore, $B = 0$. In this case, we find that $\alpha = \pm 1$ is again the correct solution. The plus or minus signs in Eq. (81) indicate that a positive or negative moment on the cylinder will make no difference so far as buckling is concerned. Eq. (81) indicates that the sandwich cylinder buckles when the maximum bending stress reaches the buckling stress when the cylinder is under axial compression only.

Case 4. Buckling under combined axial compression and bending

The determination of the buckling load for a sandwich cylinder under combined compression and bending can be carried out in a manner similar to that employed in the case of buckling under pure bending. Let $T = 0$ in Eqs. (54) and (55). Again, by assuming large λ, Eqs. (54) and (55) become

$$K_{n-1} + L K_n + K_{n+1} = 0 \qquad (82)$$

for $n \neq 1$, where $L' = \left[1 - (N_1/C) \right] IC/Mat$. For $n = 0$, we have

$$L' K_0 + K_1 = 0 \tag{83}$$

and, for $n = 1$, we have

$$2K_0 + L' K_1 + K_2 = 0 \tag{84}$$

Eqs. (82), (83), and (84) are exactly the same as Eqs. (74), (75), and (76). The solution is therefore $L' = \pm 2$ or

$$N_1 \pm (2Mat/I) = C = (h+t)G_c \tag{85}$$

Equation (85) again indicates that buckling of the sandwich cylinder will occur when the maximum compressive stress in the cylinder is equal to the buckling stress when the cylinder is under compression alone.

Case 5. Buckling under combined axial compression and torsion

When $M = 0$ and again assuming that λ is large while the ratio n/λ may be finite, Eqs. (54) and (55) become

$$\left(1 + \frac{n^2}{\lambda^2} - \frac{N_1}{C} - \frac{T}{\pi a^2 C} \frac{n}{\lambda}\right) K_n = 0 \tag{86}$$

and

$$\left(1 + \frac{n^2}{\lambda^2} - \frac{N_1}{C} + \frac{T}{\pi a^2 C} \frac{n}{\lambda}\right) K_n' = 0 \tag{87}$$

The non-trivial solution occurs when

$$\frac{T}{\pi a^2 C} \frac{n}{\lambda} = \pm \left(1 + \frac{n^2}{\lambda^2} - \frac{N_1}{C}\right) \tag{88}$$

Minimizing T or N_1 with respect to the ratio (n/λ), we find

$$\frac{n}{\lambda} = \pm \frac{T}{2\pi a^2 C}$$

and buckling occurs when

$$\left(-\frac{T}{2\pi a^2 C}\right)^2 + \frac{N_1}{C} = 1 \tag{89}$$

or

$$\frac{T}{2\pi a^2 C} = \pm\sqrt{1 - \frac{N_1}{C}} \tag{90}$$

Case 6. Buckling under combined axial compression, bending and torsion.

Now let us take up the general case of buckling under combined compression, bending and torsion. Our problem is then to find the non-trivial solutions of Eqs. (54) and (55). This is, however, a very difficult task. From the previous cases of buckling of sandwich cylinders with weak core under compression alone, bending alone, and torsion alone, it was found that the minimum buckling loads occur at $\lambda = \infty$. Dividing equations (54) and (55) by λ^8, and remembering that n_1 may also be very large, we shall drop all terms containing λ to a power greater than zero in the denominator but keep terms containing the ratio n_1/λ . Equations (54) and (55) thus become

$$\left(1 + \frac{n^2}{\lambda^2} - \frac{N_1}{C} - \frac{T}{\pi a^2 C}\,\frac{n}{\lambda}\right) K_n + \frac{Mat}{IC}\left(K_{n-1} + K_{n+1}\right) = 0 \tag{91}$$

$$\left(1 + \frac{n^2}{\lambda^2} - \frac{N_1}{C} + \frac{T}{\pi a^2 C}\,\frac{n}{\lambda}\right) K'_n + \frac{Mat}{IC}\left(K'_{n-1} + K'_{n+1}\right) = 0 \tag{92}$$

or, dividing these equations through by Mat/IC, we obtain

$$K_{n+1} + L_n K_n + K_{n-1} = 0, \tag{93}$$

$$K'_{n+1} + L'_n K'_n + K'_{n-1} = 0 \tag{94}$$

in which

$$L_n = \frac{IC}{Mat}\left(1 + \frac{n^2}{\lambda^2} - \frac{N_1}{C} - \frac{T}{\pi a^2 C}\,\frac{n}{\lambda}\right), \tag{95}$$

$$L'_n = \frac{IC}{Mat}\left(1 + \frac{n^2}{\lambda^2} - \frac{N_1}{C} + \frac{T}{\pi a^2 C}\,\frac{n}{\lambda}\right) \tag{96}$$

As in cases 3 and 4, one may attempt to solve equations (93) and (94) as finite-difference equations. This, however, was not found possible. The reason is that equations (93) and (94) are now finite-difference equations with variable coefficients and the solutions of such equations are difficult mathematical problems. Instead we shall solve the problem in the following manner.

Let us first investigate the magnitude of n_1. If n_1 is small compared to λ then $n_1/\lambda \longrightarrow 0$ as $\lambda \longrightarrow \infty$ and equations (93) and (94) reduce to the governing equations in the case of combined compression and bending. In order that the torsional load may have any effect on the buckling phenomena, n_1 must also be a large number so that the ratio n_1/λ may remain finite. For any n close to n_1, say, $n = n_1-1, n_1-2, \ldots, n_1-q$, $(q \ll n_1)$, it is obvious that such terms as $1/\lambda$, $2/\lambda$, . . . q/λ vanish as $\lambda \longrightarrow \infty$. Thus, for the equations in which $n = n_1, n_1-1, n_1-2, \ldots, n_1-q$, the following relations hold:

$$\begin{aligned} L_{n_1} &= L_{n_1-1} = L_{n_1-2} = \ldots = L_{n_1-q} \\ &= \frac{IC}{Mat}\left(1 + \frac{n_1^2}{\lambda^2} - \frac{N_1}{C} - \frac{T}{\pi a^2 C}\,\frac{n_1}{\lambda}\right) \\ &= \bar{L} \end{aligned} \tag{97}$$

Therefore, if in the series for w we take the summation of terms from n_1-q to n_1, the system of equations will be as follows:

$$\left.\begin{aligned} \bar{L}K_{n_1} + K_{n_1-1} &= 0 \\ K_{n_1} + \bar{L}K_{n_1-1} + K_{n_1-2} &= 0 \\ &\ldots \\ K_{n_1-q+1} + \bar{L}K_{n_1-q} &= 0 \end{aligned}\right\} \tag{98}$$

and

$$\left.\begin{aligned} \bar{L}'K'_{n_1} + K'_{n_1-1} &= 0 \\ K'_{n_1} + \bar{L}'K'_{n_1-1} + K'_{n_1-2} &= 0 \\ \cdots & \\ K'_{n_1-q+1} + \bar{L}'K'_{n_1-q} &= 0 \end{aligned}\right\} \qquad (99)$$

where $\bar{L}' = \frac{IC}{Mat}\left(1 + \frac{n_1^2}{\lambda^2} - \frac{N_1}{C} + \frac{T}{\pi a^2 C}\,\frac{n_1}{\lambda}\right)$

To obtain the non-trivial solution of (98) we set the determinant of the coefficients K_n equal to zero, namely,

$$\begin{vmatrix} \bar{L} & 1 & 0 & 0 & 0 \cdots 0 & 0 \\ 1 & \bar{L} & 1 & 0 & 0 \cdots 0 & 0 \\ 0 & 1 & \bar{L} & 1 & 0 \cdots 0 & 0 \\ & & & \cdot & & \\ & & & \cdot & & \\ & & & \cdot & & \\ 0 & 0 & 0 & 0 & 0 \cdots 1 & \bar{L} \end{vmatrix} = 0 \qquad (100)$$

Equation (100) can be rewritten as

$$\bar{L} - \cfrac{1}{\bar{L} - \cfrac{1}{\bar{L} - \cdots - \cfrac{1}{\bar{L} - \cfrac{1}{\bar{L} - \cfrac{1}{\bar{L}}}}}} = 0 \qquad (101)$$

By taking more and more terms in the expression for w, we have successively larger and larger continued fractions in (101) and in each case the roots $\bar{L}$ are found.

The question now arises as to which of the roots obtained in solving equation (101) is the one which should be used in the final analysis. This is easily determinable from relation (97), which, when rewritten, becomes

$$M = \frac{IC}{\bar{L}at}\left(1 + \frac{n_1^2}{\lambda^2} - \frac{N_1}{C} - \frac{T}{\pi a^2 C}\,\frac{n_1}{\lambda}\right) \tag{102}$$

Obviously the lowest value of the critical bending moment M occurs for the largest value of $\bar{L}$; therefore, in solving equation(101), the largest root obtained in each case is the one selected.

It is noted (Fig. 9) that the largest root of equation (100) approaches the value of 2.00 as larger and larger continued fractions are considered. Therefore the value $\bar{L} = 2.00$ is taken as the solution. Equation (102) therefore becomes, after dividing through by $IC/\bar{L}at$,

$$\frac{2Mat}{IC} = 1 + \frac{n_1^2}{\lambda^2} - \frac{N_1}{C} - \frac{T}{\pi a^2 C}\,\frac{n_1}{\lambda}. \tag{103}$$

In order to find the lowest possible value of the term $2Mat/IC$, it is necessary to minimize the right-hand side of (103) with respect to the variable n_1/λ. Thus, we obtain

$$\frac{\partial}{\partial(n_1/\lambda)}\left(1 + \frac{n_1^2}{\lambda^2} - \frac{N_1}{C} - \frac{T}{\pi a^2 C}\,\frac{n_1}{\lambda}\right) = 0. \tag{104}$$

Hence

$$\frac{n_1}{\lambda} = \frac{T}{2\pi a^2 C} \tag{105}$$

Consequently, equation (103) becomes

$$\frac{2Mat}{IC} = 1 - \frac{N_1}{C} - \left(\frac{T}{2\pi a^2 C}\right)^2 \tag{106}$$

or

or

$$\frac{T}{2\pi a^2 C} = \pm \sqrt{1 - \frac{N_1}{C} - \frac{2Mat}{IC}} \tag{107}$$

Exactly the same result is obtained if the non-trivial solution is found from equation (92). It is to be noted that the buckling loads in Cases 1 to 5 can all be obtained from eq. (107), as they should be.

If we define the stress ratios R_C, R_B, R_T according to the following formulas

$$R_C = \frac{N_1}{C} = \frac{\text{Critical compressive stress}}{\text{Buckling stress under compression alone}}$$

$$R_B = \frac{2Mat}{IC} = \frac{\text{Critical bending moment}}{\text{Buckling moment under bending alone}}$$

$$R_T = \frac{T}{2\pi a^2 C} = \frac{\text{Critical torsional moment}}{\text{Buckling moment under torsion alone}}$$

then equation (105) may be written as

$$R_T = \pm \sqrt{1 - (R_B + R_C)}. \tag{108}$$

The interrelationship between compression, bending, and torsional stress ratios given by equation (108) is plotted for engineering use in Figs. 10 and 11. Once any two stress ratios are specified, the buckling value of the remaining stress ratio can be determined graphically from these curves.

Experimental Investigation*

Case 1. Buckling Under Axial Compression

Test program.

In an effort to test cylinders within a range of practical interest, it is desirable that the radius to thickness ratio should be as large as possible. Whereas a relatively large value of the a/t parameter is easily obtainable for a homogeneous cylinder by constructing the cylinder of sheet of several thousandths of an inch thickness, the sandwich cylinder presents the problem that considerably greater thickness is required for the sandwich for practical reasons.

A 1/8-in. thick sandwich was considered the minimum thickness feasible, and consequently rather large radii were chosen so that the a/t values would be within a range of possible use in aircraft construction. Three different radii were used to permit a variation in the a/t parameter to be studied within the capacity of the testing facilities. To determine the length effect, if any, two different lengths were used in the investigations.

All other details of the specimens were similar. The 24S-T aluminum-alloy faces of 0.010-in. thickness were bonded to a 1/8-in. cellular cellulose acetate (CCA) core of approximately 4.5 to 5.0 lbs. per cu. ft. density. At each end of the cylinder, a 1 1/2-in. deep hardwood insert replaced the core to allow for the uniform introduction of end loads into the cylinder.

The cylinders were manufactured by Skydyne, Inc., Port Jervis, N.Y., and their fabrication details are quoted: "All aluminum faces are coated with a metal primer prior to assembly to the core. The primer is an adhesive manufactured by the Casein Company of America and bears their code number of NT-442.

---

* The experimental work was carried out mostly by G. Gerard and F. K. Teichmann.

The core is then planed to the thickness of 1/8 in., and solid wood reinforcements are glued to the edge. A secondary adhesive is used to combine the aluminum faces and the core; the adhesive used is Plastron 250-2. Although this resin adhesive will polymerize at a room temperature of 75°F., sufficient heat was applied during the fabrication of the cylinders to accelerate the "setting" of the bond. Pressure necessary to bring the surfaces in intimate contact was applied, and the assembly was molded in a period of 2 to 3 hours. The final operation consists of trimming or finishing the ends of the cylinder to assure an even plane and squareness to the ends."

Load was applied to each speciment by means of a Baldwin-Southwark universal hydraulic testing machine. The 10-in. radius cylinders were tested in a machine of 60,000-lb. capacity, whereas the remainder were tested in a 200,000-lb. capacity machine. The specimen rested on a 1/4-in. machined plate, which in turn rested directly on the base of the machine. A 1 1/2-in. machined steel plate was centered on top of the cylinder and load was applied to this through a self-aligning compression head.

During the progress of the test, load was applied slowly. At appropriate increments of load, strain-gage readings at four stations and deflection readings at three stations were taken. Near the buckling load of the cylinder, the load increments were reduced. At failure, both the maximum load and the drop load at which the machine stabilized were recorded.

Ultimate loads and dimensions

A summary of the important test results is given in Table 2. The various dimensions given in this table are those that were obtained prior to test at the estimated center of the buckle pattern. It was noted, however, that this location usually did not coincide with the location of minimum thickness or maximum length of the cylinder.

Table 2

Presentation of Test Data

Cylinder*	Nominal Length, In.	Inside Radius, In.	Total Thickness, In.	Face Thickness, In.	Calculated Core Thickness, In.	Ultimate Load, Lbs.	Drop Load, Lbs.
1012A+	12	10.05	0.144	0.0107	0.1226	9,675	4,225
1012B	12	9.99	0.134	0.0107	0.1126	11,825	4,025
1024A	24	10.09	0.138	0.0107	0.1166	10,625	5,025
1024B	24	10.05	0.135	0.0107	0.1136	13,985	5,625
1212A	12	12.00	0.142	0.0107	0.1206	18,175	5,675
1212B	12	11.89	0.136	0.0107	0.1146	18,475	8,950
1224A	24	11.88	0.132	0.0107	0.1106	17,625	8,225
1224B	24	Premature failure due to poor bonding					
1412A	12	13.89	0.143	0.0107	0.1216	26,950	2,250
1412B	12	13.86	0.134	0.0107	0.1126	33,800	2,400
1424A	24	13.88	0.132	0.0107	0.1106	21,150	5,900
1424B	24	13.84	0.131	0.0107	0.1096	18,450	7,100

* Note that the cylinders are identified by the radius that is given by the first two digits and the length that is given by the last two digits.

\+ This cylinder was initially buckled, during manufacture, at the location of buckling under load.

Material property tests conducted on the CCA core material indicated that a shear modulus of G_c = 2,000 lbs. per sq. in. $\pm$ 20 per cent was a representative value. Since the stress in the faces at buckling was well below the proportional limit of the material, no material property tests were conducted on the face material.

Description of failure

In general, the mode of instability observed on the cylinders tested can be roughly divided into three groups: (a) Cylinders in which buckles appeared in isolated locations before snap buckling precipitated failure; 1012A, 1012B, 1212B. (b) Cylinders in which no visible evidence

of buckling occurred before snap buckling precipitated failure: 1024A, 1024B, 1212A, 1224B. (c) Cylinders in which outward bulging either preceded or accompanied snap buckling: 1412A, 1412B, 1424A, 1424B.

The cylinders in group (a) exhibited isolated buckles that grew as the load was increased. These buckles usually formed the nucleus of the snap buckle pattern that occurred at failure with explosive violence. At failure, the ultimate load dropped to a value approximately 40 per cent of the peak value. The behavior of group (b) was similar with respect to the drop in load. The characteristic buckle pattern obtained in these groups is shown in Fig. 12.

Group (c) cylinders exhibited a short wave length outward bulge, usually at the junction of the CCA core and hardwood insert, in addition to a snap buckling pattern. The former mode of instability appeared to be characteristic of the type associated with wrinkling of the faces. In the cases where the outward bulging preceded failure, it was noticed that portions of the bulge area changed to the characteristic snap buckle pattern at, or immendiately after, failure. In addition, the drop load was much less than for the other two groups, averaging about 20 per cent of the peak value.

Buckle patterns

Data on the buckle patterns obtained in the tests are given for each cylinder in Table 3.

The shapesof the buckles obtained from the snap buckle patterns were diamond-shaped as shown in Fig. 12 and of approximately 3 to 1 aspect ratio as given in Table 3. They indicated the characteristic tendency to buckle inwardly. It is noted for purposes of comparison that, for a homogeneous cylinder, the buckle is usually diamond-shaped and of an aspect ratio close to unity.

Another detail of importance was the occurrence of only one buckle in the axial direction for all the cylinders. In testing Cylinders 1012B and 1024A, excessive deformation was applied to the cylinder to de-

termine if additional buckles would form in the axial direction. It was observed that no further buckling occurred. This behavior is probably due to the formation of a weak area at the buckle location once buckling occurs. Further deformation of the cylinder appears to be completely restricted to the buckle location with ultimate crushing of the core and separation between the face and core.

Table 3

Data on Buckle Patterns

Cylinder	Buckle Size: Longitudinally $L_x = \lambda/m$ in.	Buckle Size: Circumferentially $L\theta = \frac{\pi a}{n}$ in.	Number of Circumferential Buckles*	$\frac{L\theta}{L_x} = \frac{\lambda}{n}$
1012A	1.5	4.0	24	2.67
1012B	1.5	4.0	24	2.67
1024A	1.5	4.0	24	2.67
1212A	1.5	4.5	24	3.00
1224A	1.5	4.5	24	3.00

* Note that these buckles were sinusoidally arranged around the circumference (see Fig. 1[illegible]).

Influence of length

A 12-and 24-in. length of each cylinder were included in the test program to determine the influence of length upon the buckling characteristics within this range of length. Allowing for the hardwood inserts in the end of each specimen, the free length, L_f, of the cylinders in which buckling is likely to occur is reduced to 9 and 21 in., respectively.

The buckling load per inch, N_{cr}, as a function of L_f/a is shown in Fig. 1[illegible]. Within this range of the parameter and considering the scatter of the test data, no conclusions as to the effect of length could be determined. Examination of the buckle dimension data indicates, however,

that no effect of length on the buckling load should occur, since, for the shortest cylinder, the axial wave length was approximately one-sixth of the free length. It is anticipated that only when the free length approaches the axial length will the length influence the buckling characteristics.

Physical and material property variation

Examination of the dimensional properties of each cylinder indicated that the variation in dimensions from the average were of the following approximate orders of magnitude: (a) face thickness, $t \pm 0.0015$ in. (commercial tolerance); (b) core thickness, $h \pm 0.008$ in.; (c) inside radius; $a \pm 0.030$ in.; (d) length, $\lambda \pm 0.008$ in.

Variation in the shear modulus of the CCA core was found to be $G_c \pm 20$ per cent. The variation of E_f of the face material is known to be negligible for aluminum alloys. A value of $E_f = 10.5 \times 10^6$ lbs. per sq. in. was used.

An attempt was made to correlate the location estimated to be responsible for buckling with initial imperfections such as minimum values of thickness or maximum values of length. From the tabulation of dimensional data for each of the cylinders, no correlation was indicated. Since correlation with dimensional imperfections was lacking, it is assumed that the buckle location is caused primarily by local weak spots created by the variations in the core shear modulus. The fact that only one longitudinal buckle formed in all cylinders appears to be further confirmation of this hypothesis.

Additional evidence of this type of behavior of sandwich elements subject to buckling has previously been offered by Hoff and Mautner[12]. They suggest that, in a sandwich structure subject to uniform load, such as a beam in bending, the results are a statistical average of the core properties. On the other hand, a structure subject to buckling responds to local weak spots caused by defects in the core properties, and, hence, the results should be based on the lowest properties rather than on the average properties.

Correlation of theory and test data

It was found herein that for values of $E_f t/G_c a \geq 0.95$, the critical loading is given by the following equation:

$$N_{cr} = (h + t)\, G_c$$

It appears that, for this range of $E_f t/G_c a$, the critical stress is independent of the radius a and depends essentially upon the core properties.

To test the validity of this conclusion, the test data are plotted in Fig. 14 as a function of a. Also shown are the results obtained from the preceding equation based on the upper and lower limits of the shear modulus, G_c, given previously. Since no correlation of failure location with dimensional imperfections was obtained as discussed in the previous section, it is assumed that the variation in the shear modulus is primarily responsible for buckling.

While the test data in Fig. 14 appear to indicate an apparent influence of the radius, it is felt that this apparent effect can be explained by the variation in the shear modulus. Consideration must also be given to the fact that the 10-in. radius cylinders were tested in a 60,000-lb. capacity testing machine, whereas the remainder were tested in a 200,000-lb. machine. This may have some bearing on the lower values of the 10-in. radius group. Furthermore, the cylinders were manufactured in order of increasing radius, and, if some allowance is made for an improvement in manufacturing technique with experience, then the large radius cylinders are favored.

Considering all these factors, it appears that reasonable correlation between the critical load obtained from the theory and the test data was obtained within the region of $E_f t/G_c a$ of the experiments.

Case 2. Buckling under torsion

Test program

Again the sandwich used had a thickness of 1/8 inch. The nominal radius of 6 inches which was used for all cylinders was dictated by the capacity of the testing facilities. To determine the effect of length upon the buckling load, two different lengths were used in the investigation.

The most significant parameter in overall buckling of sandwich elements is the shear rigidity of the core material. Consequently, two different materials were selected for the cores: cellular cellulose acetate (CCA) of approximately 5.5 to 6 lbs/cu. ft. density and end grain balsa (EGB) of approximately 5 to 5.5 lbs/cu. ft. density. For all cylinders, the face material used was 0.010 inch 24S-T3 aluminum alloy.

To faciltate installation of the test specimen in the loading jig, two inch wide hardwood blocks were bonded to both the inside and outside faces at each end of the cylinder (see Fig. 15). The end faces of these blocks were then turned down on a lathe to insure planeness of the face, perpendicularity with the axis of the cylinder and parallelism of the faces.

Test procedure

The pertinent dimensions of each specimen were determined as follows. Four evenly spaced longitudinal stations were lightly scribed on the outside wall of the cylinder. The outside radius was then measured to the nearest 0.01 inch at each pair of stations at both ends. The length of the cylinder between hardwood blocks was also determined at each station to the nearest 0.01 inch.

The total thickness of the cylinder wall was measured at each station at both ends just inside the hardwood blocks and at the center by means of a special dial gage with a least division of 0.001 inch. The thickness of the faces was measured with a ten-thousandths micrometer before the cylinders were assembled. The average dimensions for each cylinder are given in Table 4.

Installation of the specimens in the specially designed torsion loading jig was accomplished by bolting the specimen to the steel end plates through the hardwood blocks at the ends of the cylinder. The loading mechanism is shown in Fig. 15 with a specimen installed and tested. Load was applied by means of a hydraulic tension jack and was measured by a calibrated strain gage tension link at the jack which was accurate to $\pm$ 2 per cent.

Physical property tests

The important physical properties in overall torsional buckling of sandwich construction are the shear stress-strain characteristics of the face material and the shear modulus of the core material. The methods used to determine these properties are discussed in some detail due to their importance in evaluation of the test data.

The shear moduli of the core materials were determined by testing as simple beams, strips of flat sandwich construction. The beams were fabricated by the manufacturer of the cylinders of the same materials and in the same manner as the cylinders themselves. The test consisted of obtaining load-deflection data from which the shear modulus of the core material was determined from the difference in deflection between the experimental value and that computed for the beam neglecting shear deflections. From six tests of each core material, the following values of shear modulus were obtained:

cellular cellulose acetate: $G_c = 3400$ psi $\pm$ 20%

end grain balsa: $G_c = 15{,}700$ psi $\pm$ 7%.

No experimental technique is known for directly determining shear stress-strain characteristics of thin sheet material. The method used in this investigation was to obtain the stress-strain properties under axial compression and tension loads of specimens oriented at 45 degrees with the grain direction of the face material. This orientation was chosen since a pure shear field can be represented by orthogonal tension and compression stress of the same magnitude as the shear stress at 45 degrees with the

direction of the shear stress. The axial stress-strain data so obtained are shown in Fig. 16 as the limits of the variation in stress-strain properties from the average of the specimens tested.

A shear stress-strain curve can be constructed from axial stress-strain data by use of the following transformations of the maximum shear theory:

$$\tau = \sigma/2 \quad \text{and} \quad \gamma' = (1 + \nu)\varepsilon \tag{109}$$

In the yield region of the stress-strain curve, Poisson's ratio can be represented by[13]

$$\nu = 0.5 - 0.2\, E_s/E \tag{110}$$

where E and E_s are the elastic and secant moduli of the axial stress-strain curve. The desired shear stress-strain curve shown in Fig. 16 was obtained by applying Eqs. (109) and (110) to the upper and lower limits of the axial stress-strain data.

Test results

Average measured dimensions of the sandwich cylinders together with the failing loads are given in Table 4. Photographs of typical buckle patterns taken after conclusion of the tests are shown for each type of cylinder. Fig. 17 shows an end grain balsa core cylinder, Fig. 18 shows a CCA cylinder of 24 inch length and Fig. 19 a CCA cylinder of 12 inch length.

It is noted that in all cases, there was no observation of buckling before the failing load was reached.

Correlation of theory with experimental results

(a) End grain balsa cylinders

For this group of cylinders, we find that the parameters $E_f t/G_c a = 1.1$ and $a/(h+t) = 48$. These cylinders behave essentially as homogeneous cylinders. Therefore, the results of Ref. 14 can be used to evaluate the effect of the boundary conditions and length of the cylinder upon the critical shear stress. From Ref. 14, for a cylinder clamped at the

ends

$$\frac{\tau_{cr}(2t)\lambda^2}{\pi^2 D} = 0.93Z^{3/4} \qquad (111)$$

where D = bending rigidity of sandwich plate = $E_f t(h+t)^2/2(1-\nu_f^2)$

$$Z = \text{curvature parameter} = (1-\nu_f^2)^{1/2}\lambda^2/2at$$

In using the above relations for a sandwich plate, the thickness of the homogeneous cylinder has been replaced by twice the face thickness of the sandwich cylinder, (2t); Eq. (111) can be reduced to the following by taking $\nu = 0.3$.

$$\tau_{cr} = 1.44E_f(h+t)^2/\lambda^{1/2}(at)^{3/4} \qquad (112)$$

By substituting the appropriate values given in Table 4 for the parameters appearing in Eq. (112) it is found that

$$\tau_{cr} = 433{,}000 \text{ psi} \qquad (113)$$

The value of the critical stress given by Eq. (113) is based on elastic buckling and consequently is far in excess of the shear proportional limit of the material used. A method for computing plastic shear buckling stresses is given in Ref. 15, in which it is suggested that the effective modulus to be used in plastic shear buckling is the shear modulus. By this method, the critical shear strain is computed and the plastic buckling stress is then obtained from the shear stress-strain curve at the particular value of critical strain. From Eq. (113), therefore,

$$\gamma'_{cr} = \tau_{cr}/G_f = 0.109 \qquad (114)$$

This is evidently a very large value of critical strain for which the shear stress-strain curve is not known. In addition, it is highly doubtful that the method given in Ref. 15 (which is for the yield region of the stress-strain curve) would apply at such large values of critical strain. Therefore, to effect a comparison between theory and test data,

the test data are arbitrarily plotted in Fig. 21 at a strain of 0.01 to observe the relation between these data and the shear stress-strain curve given in Fig. 16. These data are plotted at a strain of 0.01 since this appears to be a reasonable value indicating the limit of the yield region of the stress-strain curve. Although reasonable agreement is indicated in Fig. 21 it is to be noted that significant difference between the theory and tests may be obscured by the fact that buckling occurred in the plastic region.

Table 4

AVERAGE DIMENSIONS AND FAILING LOADS OF SANDWICH CYLINDERS

Cylinder	Core Material	Length	Mean Radius	Total Thickness	Average Face Thickness	Failing Moment	Failing Load/in.	Failing Stress
		l	a	$(h+t)$	t	M_{cr}	N_{cr}	τ_{cr}
No.1	EGB	20.06"	5.99"	0.145"	0.103"	126,000"lb.	560 lb/in.	28,000psi
No.2	EGB	19.50	5.99	0.155	0.103	103,600	460	22,900
No.3	CCA	7.90	6.01	0.138	0.105	42,000	185	8,850
No.4	CCA	7.95	6.00	0.142	0.105	25,200	111	5,320
No.5	CCA	19.80	6.01	0.137	0.105	26,400	117	5,550
No.6	CCA	19.92	6.02	0.132	0.105	22,700	100	4,780

(b) Cellular cellulose acetate cylinders

The average value of the parameter $E_f t/G_c a$ for this group of cylinders was approximately five. According to Fig. 20, the buckling strength of this group of cylinders should be affected only by the shear rigidity of the core. Therefore, the experimental values of the torsional instability coefficients were computed as shown in Table 5 and plotted in Fig. 20.

Table 5

EXPERIMENTAL TORSION INSTABILITY COEFFICIENTS FOR CCA CYLINDERS

$E_f t/G_c a = 5.15$; $a/(h+t) = 48$

Cylinder	N_{cr}	$h+t$	G_c	$K_t = N_{cr}/(h+t)G_c$
No. 3	185 lb./in.	0.118"	3,400 psi	0.462
No. 4	111	0.122	3,400	0.268
No. 5	117	0.117	3,400	0.294
No. 6	100	0.112	3,400	0.263

The comparison of the theory and test data shown in Fig. 21 reveals that the test results are considerably below the theoretical value. The large variation in shear modulus of the core ($\pm$ 20%) is certainly not sufficient to account for this discrepancy. It appears, however, that poor bonding of the faces to the core may be the cause of the discrepancy.

It is possible that, because of the curvature of the structure, inspection by tapping the cylinders did not reveal any area of poor bonding before the test. During loading, however, evidences of poor bonding were noticed. The evidence was a crackling noise which was heard almost immediately upon the application of load.

Additional evidence was obtained after the cylinders were tested. In some of the cylinders, the faces were peeled from the core and it was found that there were considerable areas in which no core material remained attached to the bonding of the faces. It appears that in a satisfactory bond, particles of the core material would adhere to the bonding of the faces after peeling.

This difficulty occurred only with the CCA core material and may possibly be attributed to the small thickness (1/8") of core material used. In addition the CCA was produced by a new manufacturer and there was evidence of considerable nonuniformity of cell size.

Case 3. Buckling under bending

Test program

The cylinders tested in pure bending had again a thickness of 1/8 inch and a radius of 6 inches. To ensure uniformity of introduction of bending load, all the cylinders were 36 inches long. Two different material were again used for the core: cellular cellulose acetate (CCA) of approximately 6 lbs./cu. ft. density and end-grain balsa (EGB) of approximately 5 to 5.5 lbs./cu. ft. density. For all cylinders, the face material used was 0.010 inch 24S-T3 aluminum alloy.

To faciltate installtion of the test specimen in the loading jig, two inch wide hardwood blocks were bonded to both the inside and outside faces at each end of the cylinder (see Figs. 22 and 24). The end faces of these blocks were then turned down on a lathe to insure planeness of the face, perpendicularly with the axis of the cylinder and parallelism of the faces.

Test procedure

The pertinent dimensions of each specimen were determined as in the case of buckling under torsion. The average dimensions for each cylinder are given in Table 6.

Installation of the specimens in the specially designed bending loading jig was accomplished by bolting the specimen to the steel end plates through the hardwood blocks at the ends of the cylinder. The loading jig is shown in Fig. 22 with a specimen installed and tested. Load was applied by means of a hydraulic tension jack and was measured by a calibrated strain gage tension link at the jack which was accurate to $\pm$ 2 percent.

Physical property tests

The important physical properties in overall bending buckling of sandwich construction are the compressive stress-strain characteristics of the face material and the shear modulus of the core material.

The with-grain compressive stress-strain characteristics of the 0.010 in. 24S-T3 aluminum alloy used for the faces of the sandwich cylinders was determined by use of a solid guide compression jig of the National Bureau of Standards type. The stress-strain data are shown in Fig. 23. The shear moduli of the core materials were determined by testing as before. From at least four tests of each core material, the following values of shear modulus were obtained:

cellular cellulose acetate: G_c = 3400 psi ± 17%

end grain balsa: G_c = 17,600 psi ± 15%

Test results

Average measured dimensions of the sandwich cylinders together with the failing (buckling) loads are given in Table 6. Fig. 24 shows a typical overall buckle pattern obtained on most of the 1/8-in. cylinders; additional data on the buckling patterns are given in Table 7. The measured wavelengths were obtained in regions of relatively little distortion.

Table 6

AVERAGE DIMENSIONS AND FAILING LOADS OF SANDWICH CYLINDERS

Cylinder	Core Material	Length	Mean Radius	Total Thickness	Average Face Thickness	Failing Moment	Maximum Failing Load/in.	Maximum Failing Stress
		ℓ	a	(h+2t)	t	M_{cr}	$N_{cr}=M/\pi a^2$	σ_{cr}
No.1	CCA	32.09"	6.48"	0.141"	0.0105"	67,900"lbs.	514 lb/in.	19,300 psi
No.2	CCA	32.13	6.50	0.125	0.0105	46,100	347	16,500
No.3	CCA	32.13	6.49	0.125	0.0105	77,700	587	28,000
No.4	CCA	32.16	6.53	0.141	0.0105	89,600	670	31,900
No.5	EGB	31.29	6.47	0.141	0.0105	53,100	404	19,300
No.6	EGB	31.09	6.55	0.156	0.0105	65,700	500	23,800

Table 7

DATA ON INSTABILITY PATTERNS

Cylinder	Type of Instability	Location	Longitudinal Wave Length L_x	Circumferential Wave Length L_θ
No.1 1/8"CCA	Buckle	Central	1"	3"
No.2 1/8"CCA	Buckle	Central	1	3
No.3 1/8"CCA	Buckle	Central	1 1/4	3 1/2
	Antisymmetrical			
No.4 1/8"CCA	Wrinkle	Both ends	7/16	πa
No.5 1/8"EGB	Buckle	Central	1 1/4	3 1/2
	Antisymmetrical			
No.6 1/8"EGB	Wrinkle	At end	7/16	πa

Correlation of Theory with Experimental Results

The 1/8 in. CCA cylinders are sandwich cylinders with weak cores. The average centroidal height, (h+t), of cylinders No. 1 to No. 4 is 0.118 in. $\pm$ 6% and the average shear modulus is 3400 psi $\pm$ 17%. Therefore, the average shear rigidity of this group of cylinders is 400 lbs./in. $\pm$ 23%, which is the theoretical buckling loading. The average experimental failing loading was found to be 530 lbs./in. $\pm$ 33%. Thus, the experimental failing loading is 32 percent higher than the theoretical value, on the average.

The fact that the bending buckling load is higher than the compressive buckling load for cylinders of the same dimensions has been observed in tests on homogeneous cylinders. It has been suggested that this behavior may be due to the buckling phenomena responding to the average value of compressive stress on the cross section rather than the maximum stress. In the case of pur bending, the maximum stress would be 1.4 times as great as the average value.

For sandwich cylinders in compression, the theory indicates that the value of the parameter $E_c t/G_c a$ governs the behavior of the cylinder. Thus, it has been found that cylinders can be considered weak in

shear when the value of $E_f t/G_c a$ exceeds unity. To effect a comparison between the cylinders loaded in compression and bending which were differently constructed as concerns G_c and a, it appears that if the values of $E_f t/G_c a$ were equal or at least greater than unity for each group, a direct comparison would be valid.

The value of this parameter for the compression specimens averaged 5 and for the bending specimens $E_f t/G_c a = 5$ also. Thus, since the compressive test data checks theory very well, it can be concluded that in bending the 32% higher experimental value is in agreement with the behavior observed for homogeneous cylinders, thus accounting for the discrepancy.

Although these conclusions are based on data with which large percentage variations are associated, it appears that the trend is clearly indicated. The fact that the scatter of the experimental values is considerably higher than that for the core properties is based on the fact that the latter values were established from beam bending tests. In a beam test, the results are a statistical average of the core properties, whereas a structure subject to buckling responds to local weak spots caused by defects in the core properties. Thus, the scatter would tend to be greater for the buckling data.

The 1/8 in. end grain balsa cylinders, No. 5 and No. 6, have cores much stronger in shear than the cylinders with CCA cores. Based on the observations made on these two cylinders, it appeared that they cannot be considered in the weak in shear category. These cylinders, therefore, failed at a small fraction of the theoretical load. This is evidenced by the fact that the average failing loading of this group was 452 lbs./in. as compared to 530 lbs./in. for the 1/8 in. CCA cylinders, although the shear modulus of the EGB core was over five times as great as the CCA core. The fact that the EGB cylinders were not even as strong as the CCA cylinders is difficult to reconcile with the core properties. Unless some other mode of buckling is responsible for this anomalous behavior, it appears that poor bonding to the EGB core may be responsible for the seemingly low values of failing loading.

REFERENCES

1. Reissner, E., Small Bending and Stretching of Sandwich Type Shells, N.A.C.A. T.N. No. 1832, Mar., 1949.
2. Reissner, E., Finite Deflections of Sandwich Plates, J. of Aero. Sciences, vol. 15 No. 7, pp.435-440, July, 1948.
3. Reissner, E., Errata-Finite Deflections of Sandwich Plates, J. of Aero. Sciences, vol. 17 No. 22, p. 125, Feb., 1950.
4. Wang, C.T., Principle and Application of Complementary Energy Method for Thin Homogeneous and Sandwich Plates and Shells with Finite Deflections, N.A.C.A. T.N. No. 2620, Feb., 1952.
5. Donnell, L.H., Stability of Thin-Walled Tubes Under Torsion, N.A.C.A. Rep. No. 479, 1933.
6. Stein, M., and Mayers, J., A Small-Deflection Theory for Curved Sandwich Plates, N.A.C.A. T.N. No. 2017, Feb., 1950.
7. Wang, C.T., and Sullivan D.P., Buckling of Sandwich Cylinders Under Bending and Combined Bending and Axial Compression, J. of Aero. Sciences, vol. 19 No. 7, pp. 468-471, July, 1952.
8. Gerard, G., Torsional Instability of a Long Sandwich Cylinder, Proc. First Nat. Congress of App. Mech., A.S.M.E., pp. 391-394, June, 1951.
9. Teichmann, F.K., Wang, C.T. and Gerard, G., Buckling of Sandwich Cylinders Under Axial Compression, J. of Aero. Sciences, vol. 18 No.6, pp. 398-406, June, 1951.
10. Leggett, D.M.A., and Hopkins, H.G., Sandwich Panels and Cylinders Under Compressive End Loads, R. and M. No. 2262, British A.R.C., 1942.
11. Wang, C.T., and Rao, G.V.R., A Study of an Analogous Model Giving the Nonlinear Characteristics in the Buckling Theory of Sandwich Cylinders, J. of Aero. Sciences, vol. 19 No. 2, pp. 93-100, Feb., 1952.
12. Hoff, N.J., and Mautner, S.E., Bending and Buckling of Sandwich Beams, J. of Aero. Sciences, vol. 15 No. 12, pp. 707-720, Dec., 1948.
13. Nadai, A., Theory of Flow and Fracture of Solids, vol. I, 2nd Ed., McGraw-Hill, New York, 1950, p.387.
14. Batdorf, S.B., Schildcrout, M., and Stein, M., Critical Stress of Thin-Walled Cylinders in Axial Compression, N.A.C.A. Rep. No. 887, 1947.
15. Gerard, G., Critical Shear Stress of Plates Above the Proportional Limit, J. of App. Mech., vol. 15 No. 1, pp. 7-12, Mar., 1948.

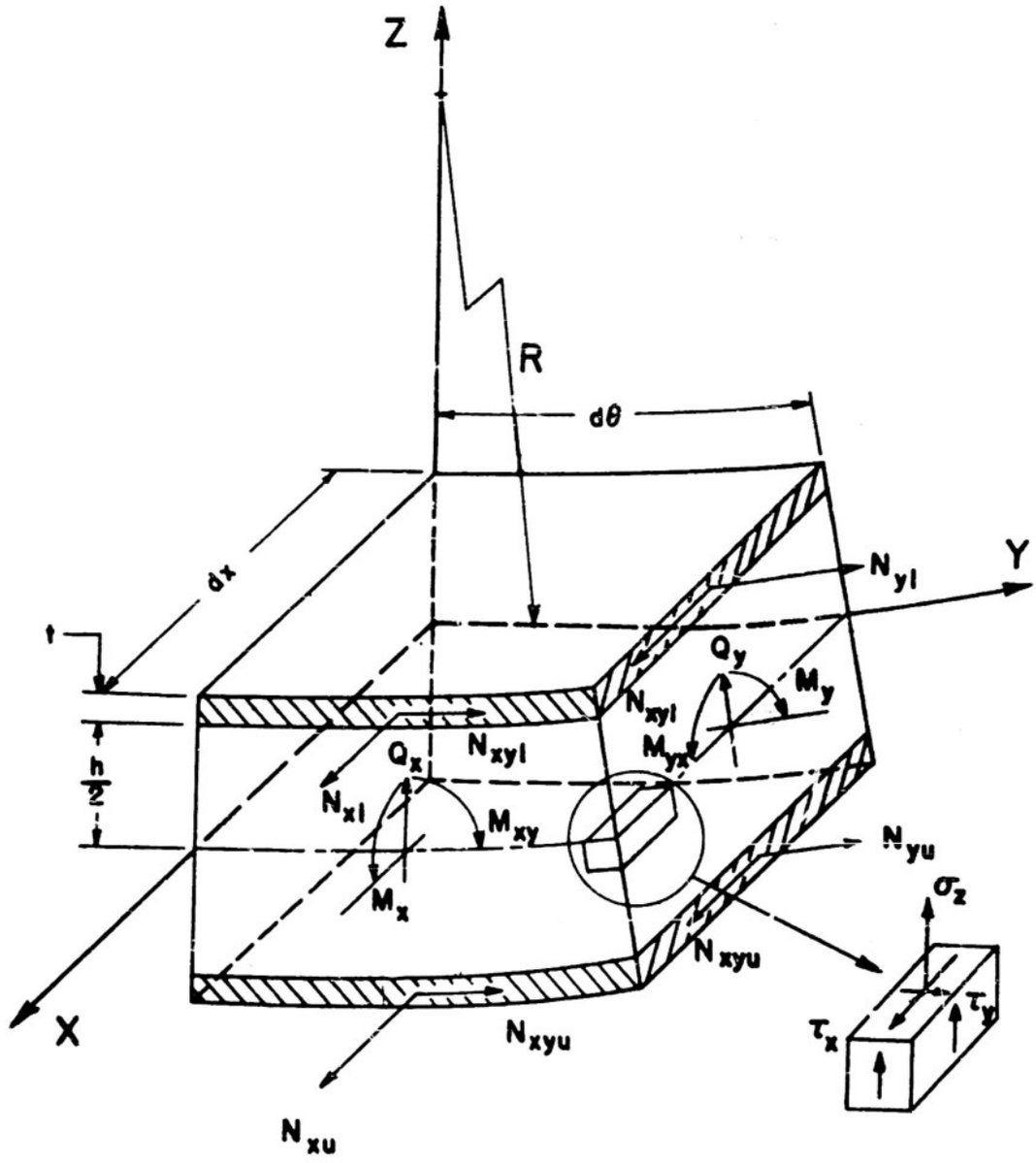

FIGURE 1. RESULTANT FORCES AND MOMENTS ACTING ON SANDWICH ELEMENT

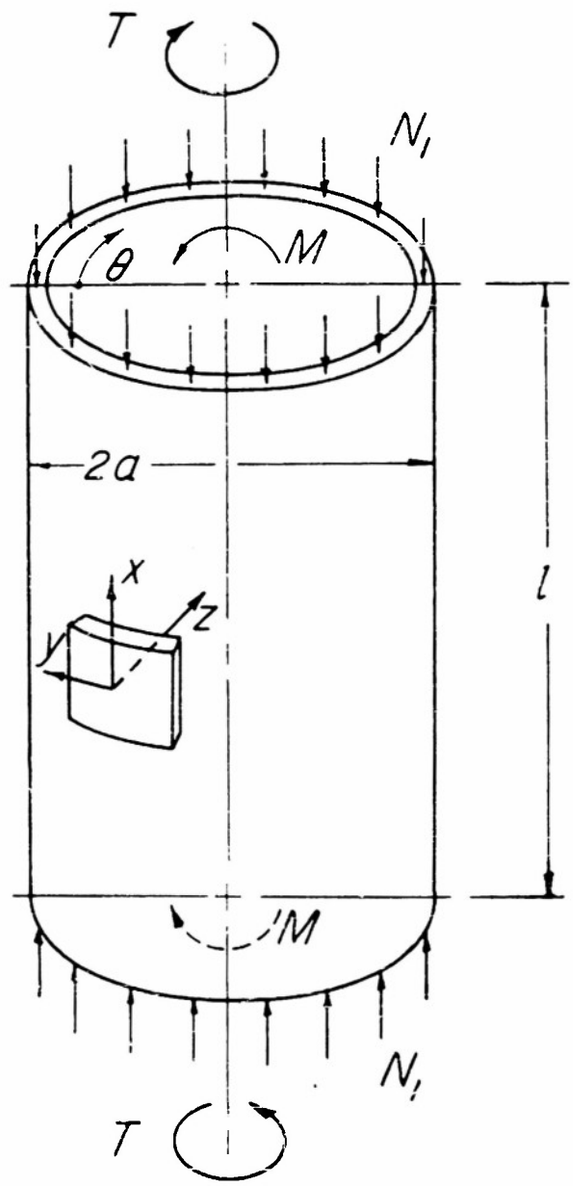

FIGURE 2. SANDWICH CYLINDER CONFIGURATION AND LOADING

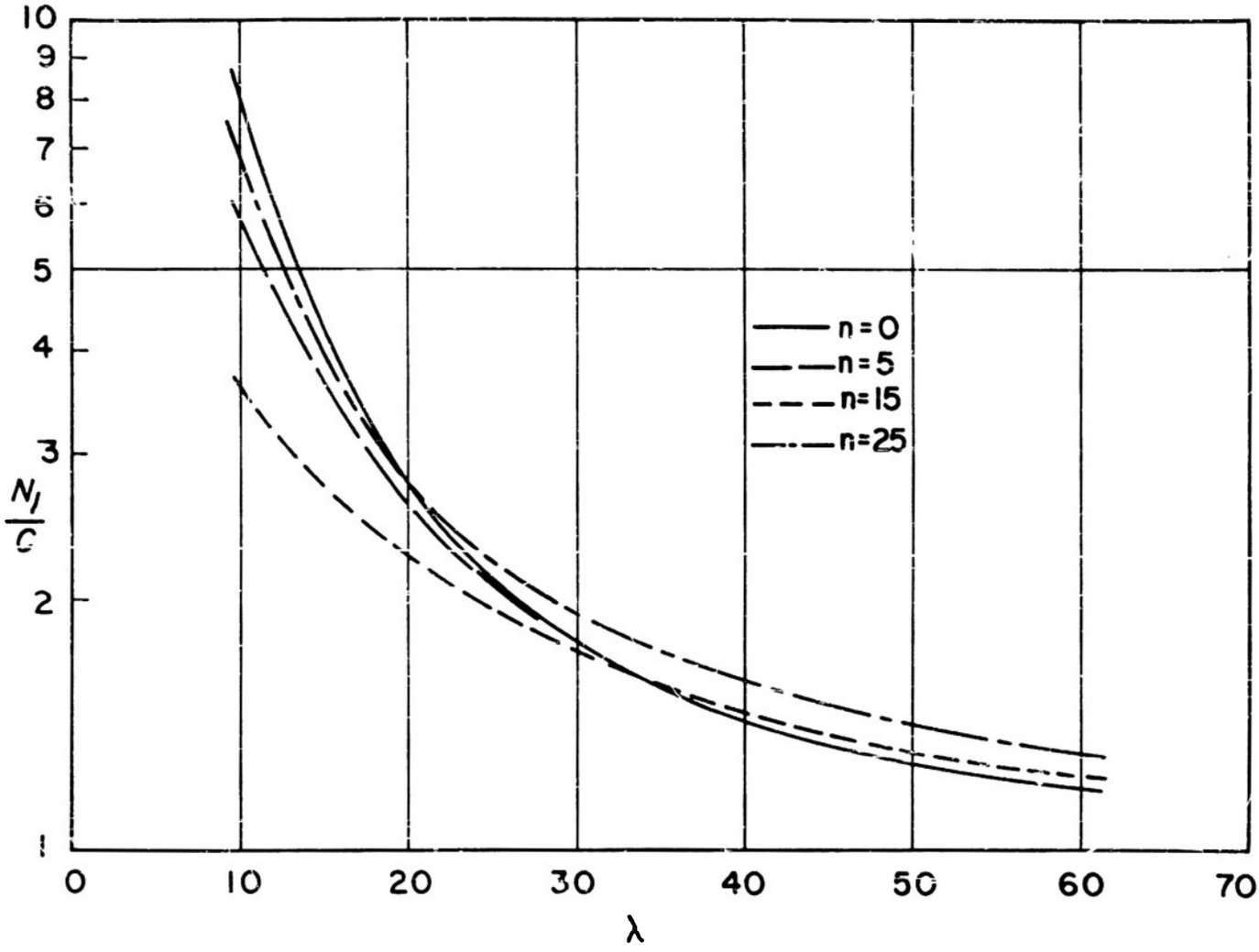

FIGURE 3. EXACT NUMERICAL RESULTS FOR CASE (a)

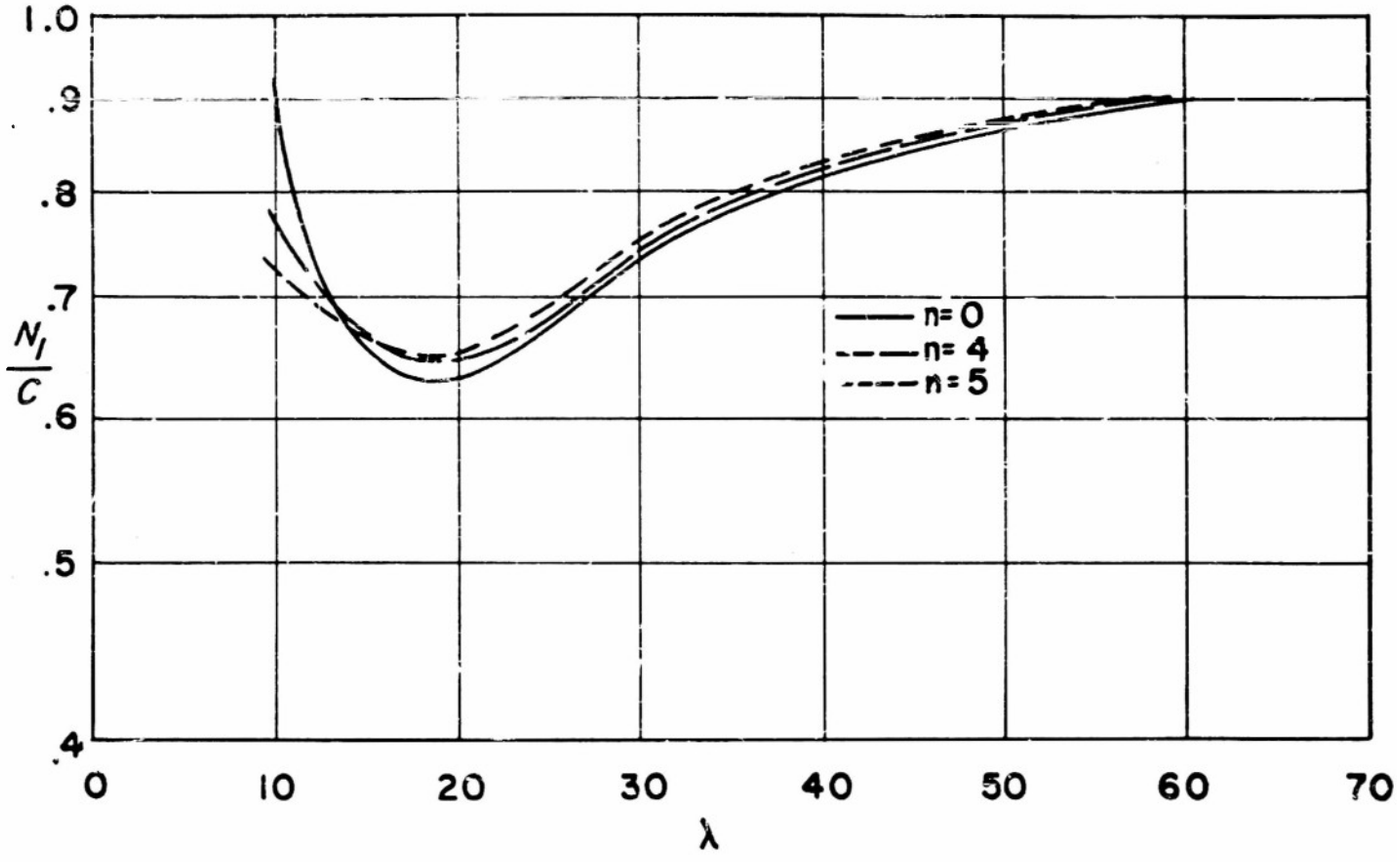

FIGURE 4. EXACT NUMERICAL RESULTS FOR CASE (b)

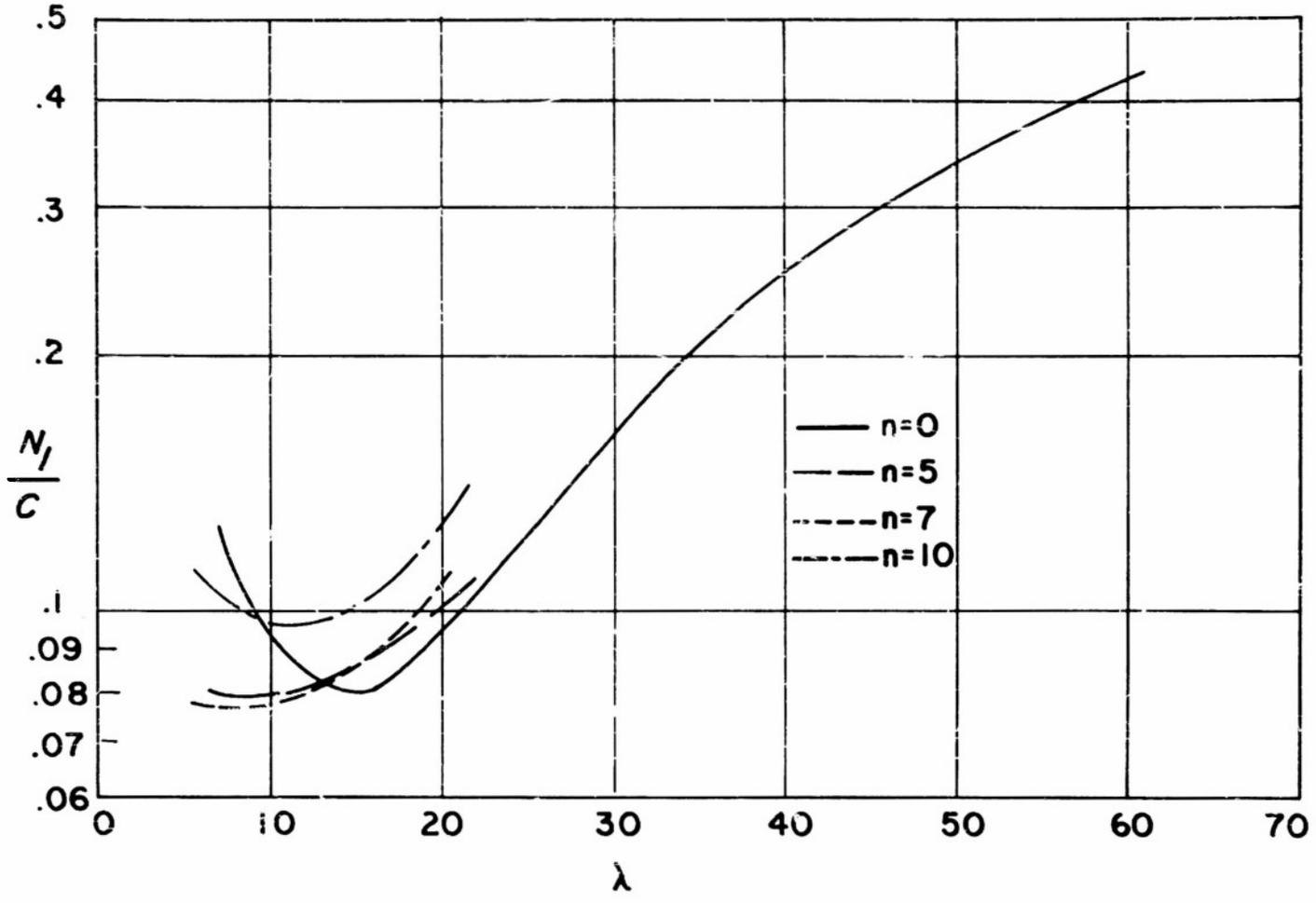

FIGURE 5. EXACT NUMERICAL RESULTS FOR CASE (c)

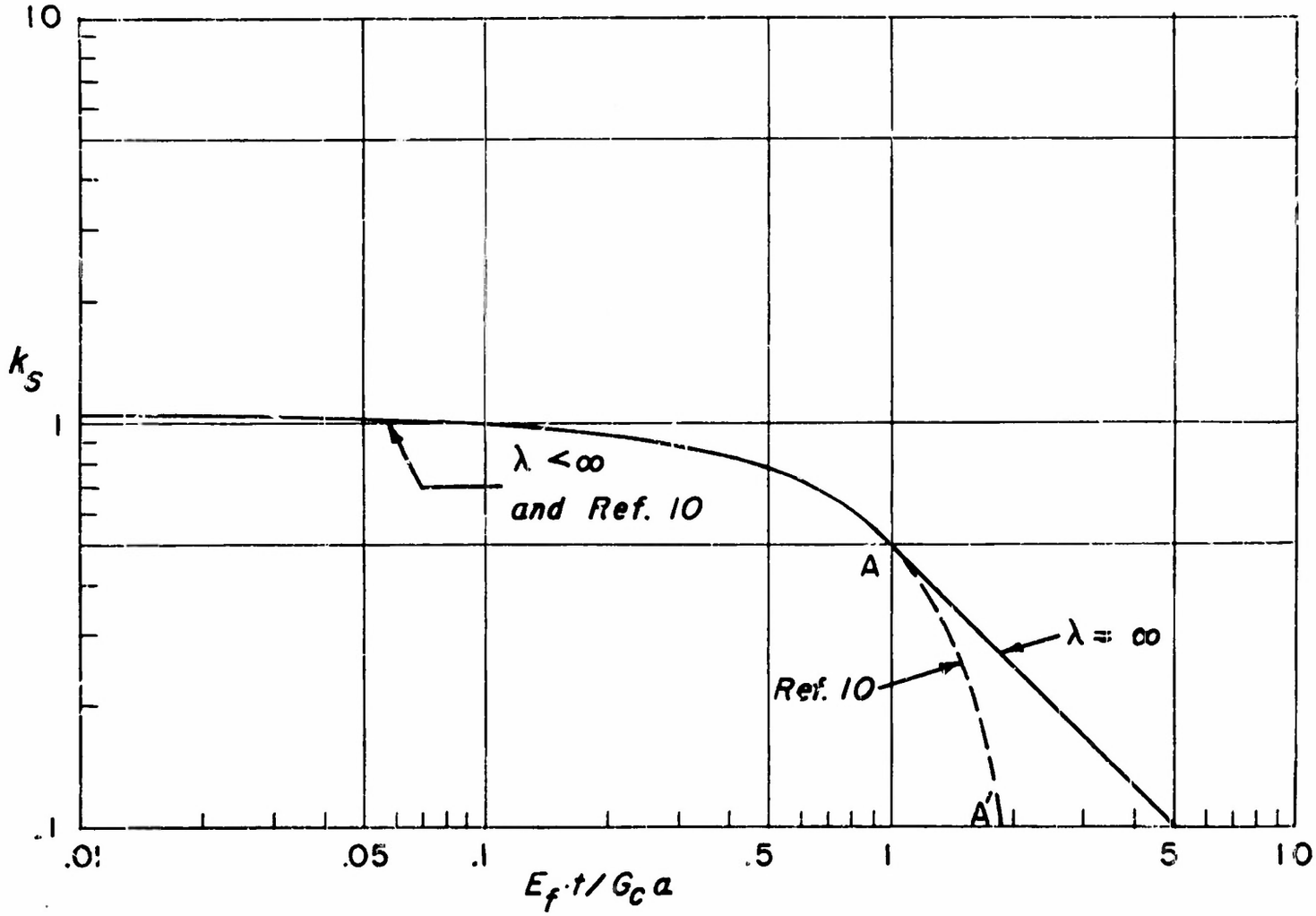

FIGURE 6. AXIAL-COMPRESSION BUCKLING COEFFICIENT

$\nu_f = 0.3$

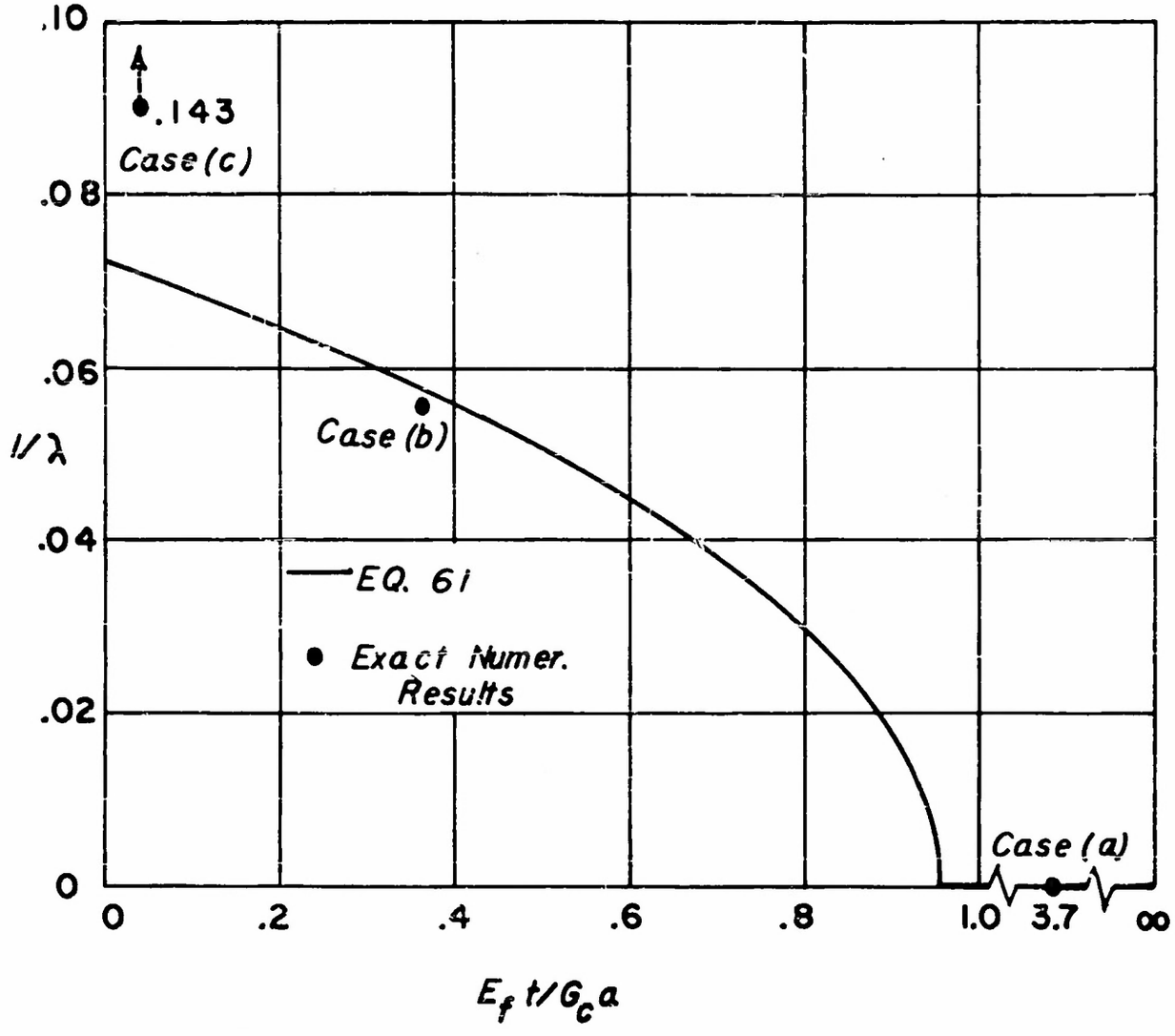

FIGURE 7. WAVELENGTH OF BUCKLING: $\nu_f = 0.3$

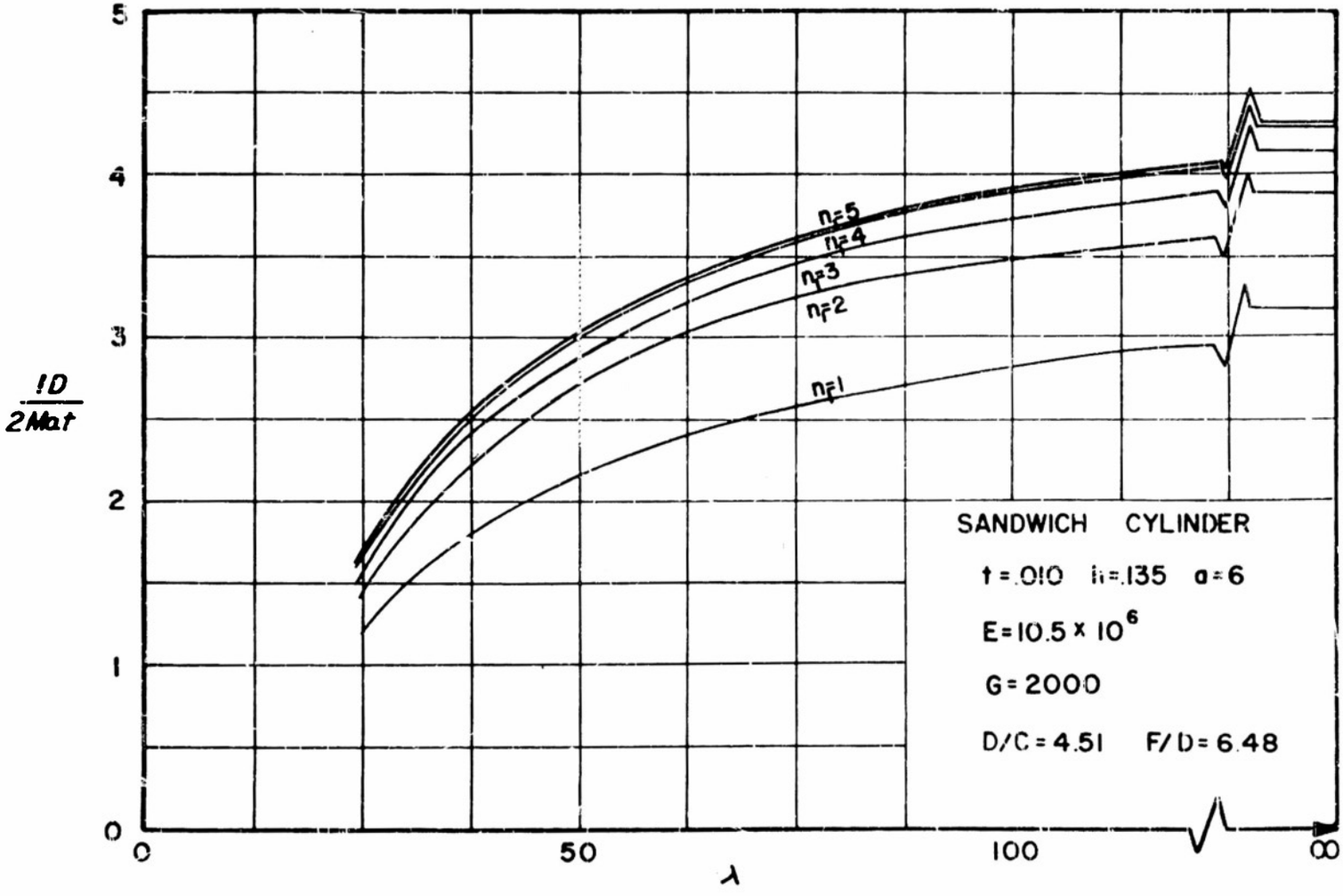

FIGURE 8. EFFECT OF λ ON THE BENDING BUCKLING LOAD

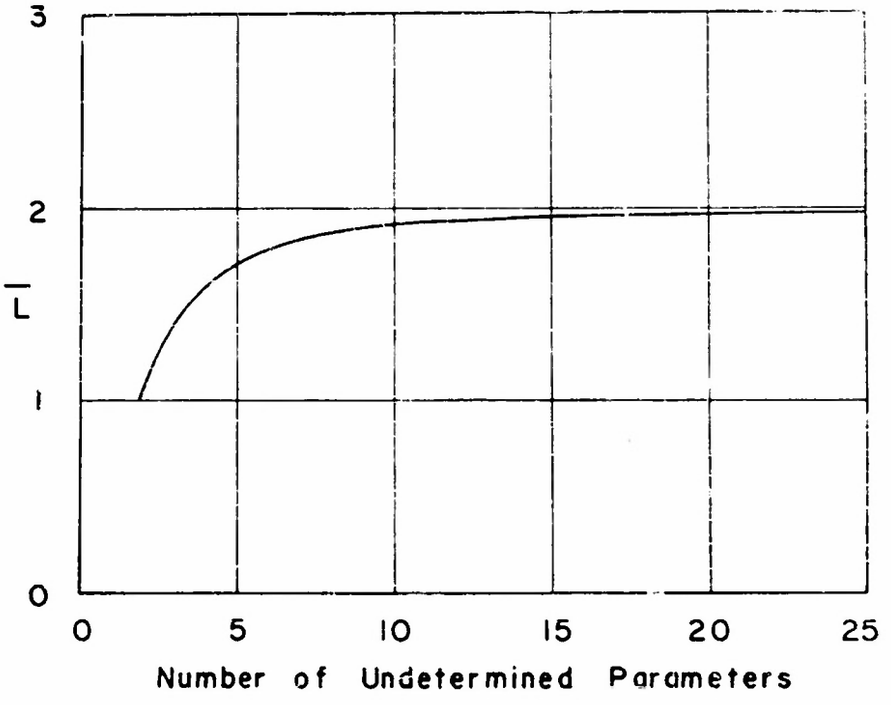

FIGURE 9. RESULT OF EVALUATING $\overline{L}$ BY METHOD OF SUCCESSIVE APPROXIMATIONS

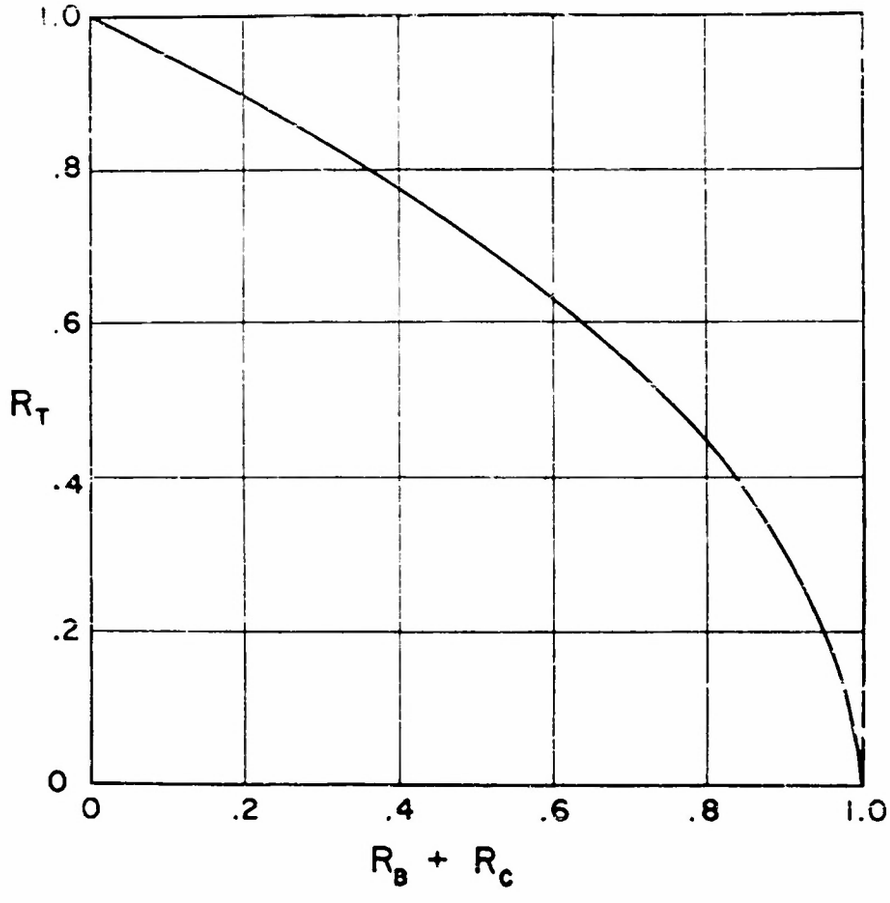

FIGURE 10. INTERACTION CURVE: TORSION STRESS RATIO vs. SUM OF BENDING AND COMPRESSION STRESS RATIOS

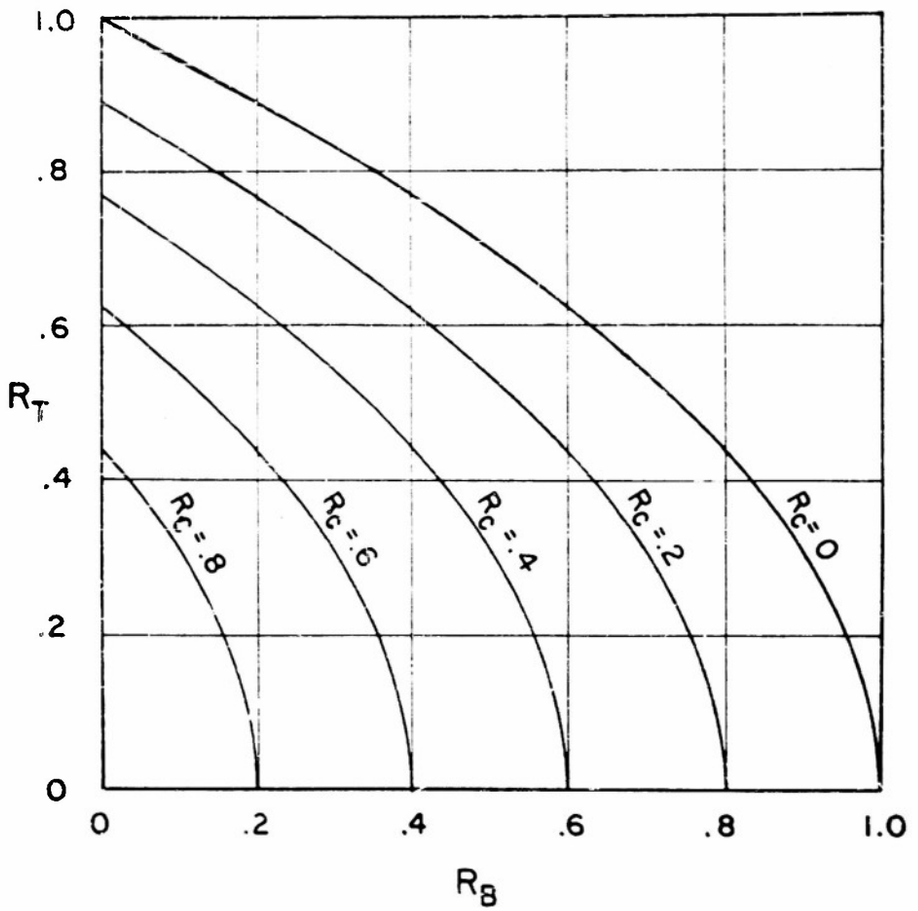

FIGURE II. INTERACTION CURVES: COMBINED LOADING

FIGURE 12. CHARACTERISTIC BUCKLE PATTERN:
1/8" CCA CYLINDER UNDER AXIAL COMPRESSION

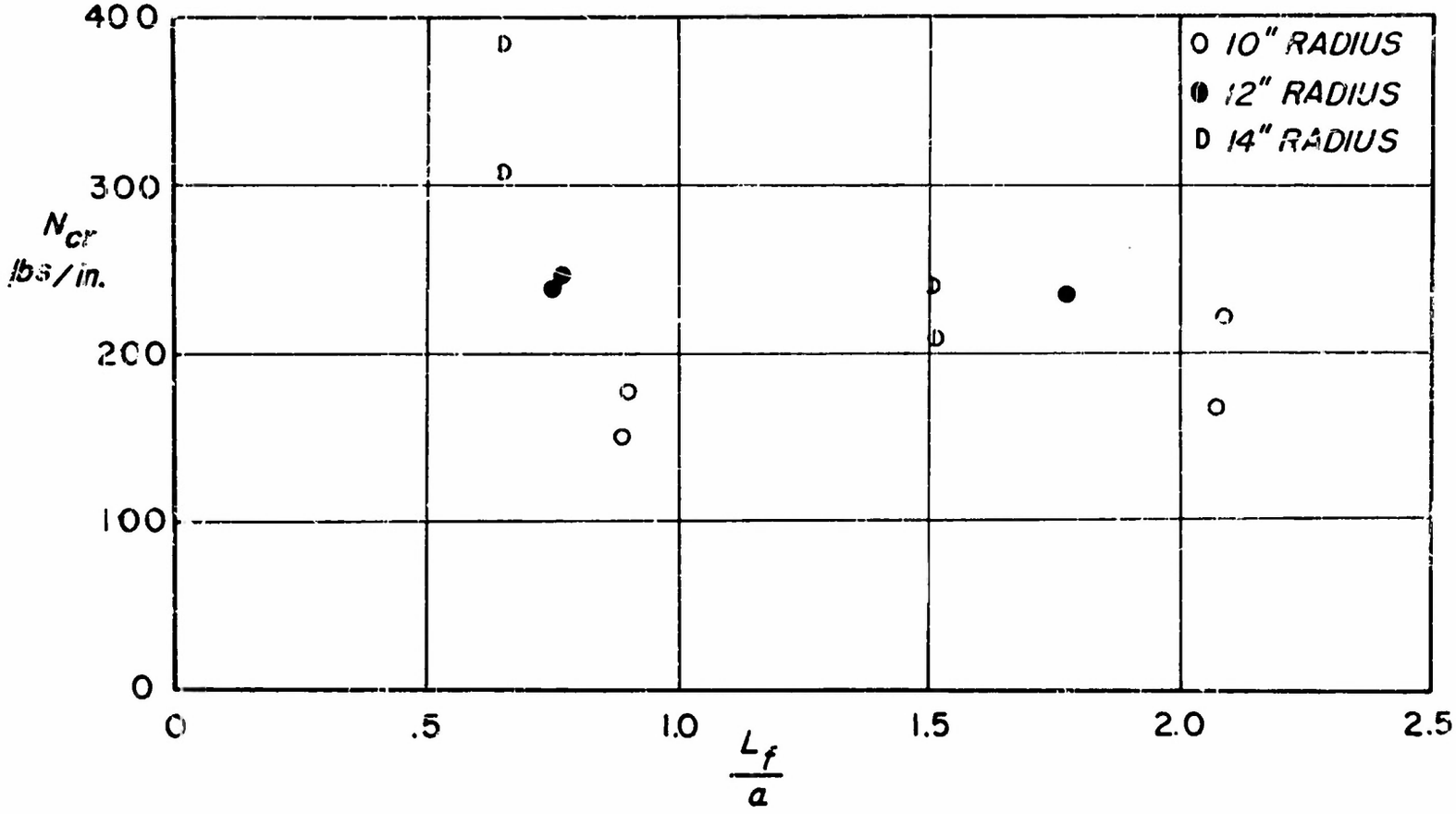

FIGURE 13. INFLUENCE OF FREE LENGTH ON FAILING LOAD

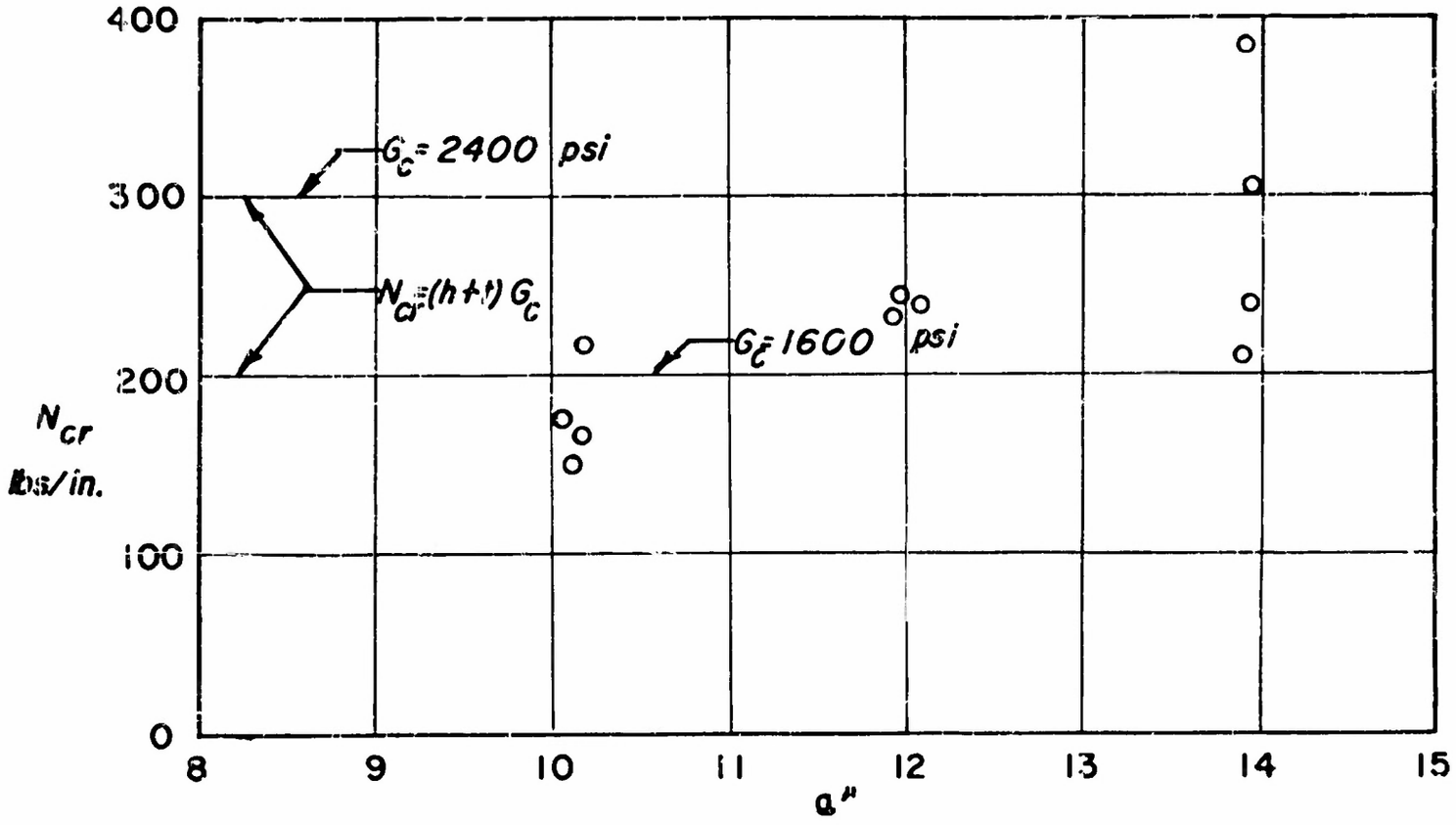

FIGURE 14. COMPARISON BETWEEN TEST DATA AND THEORY BASED ON LIMITS OF VARIATION OF G_c

FIGURE 15

TORSION TEST SET-UP

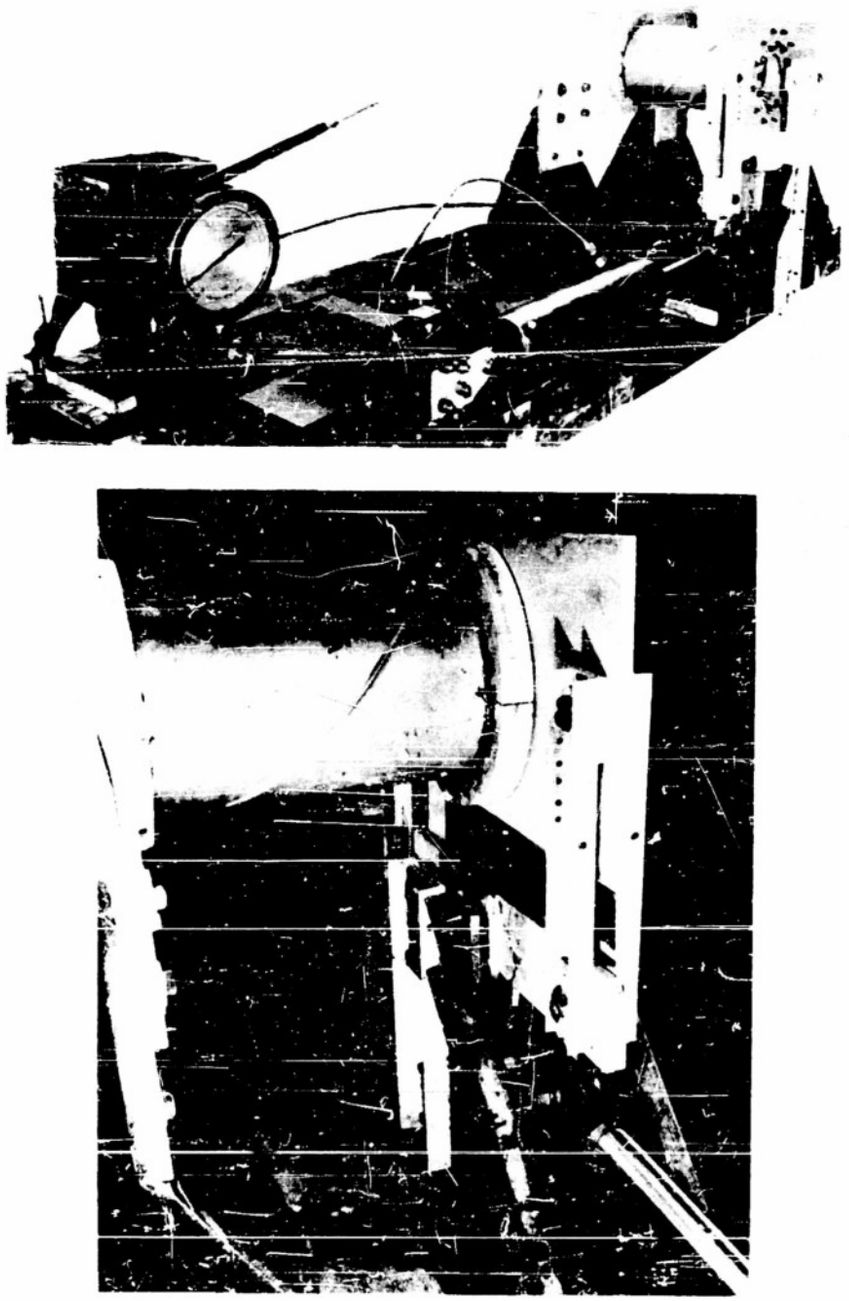

FIGURE 16. STRESS—STRAIN CHARACTERISTICS OF FACES 0.010" 24S-T AT 45° DIRECTION

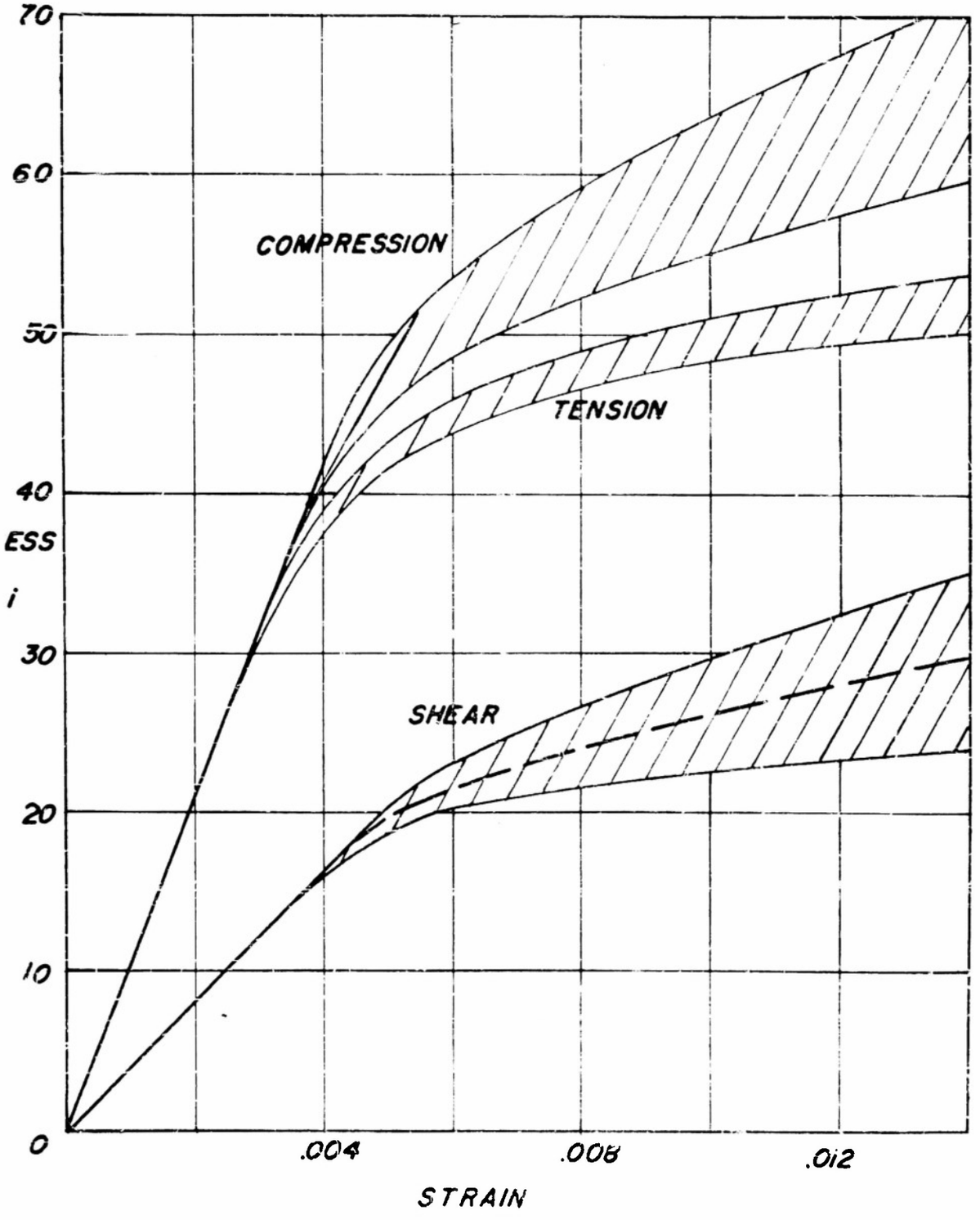

FIG. 17
24" EGB

FIG. 18
24" CCA

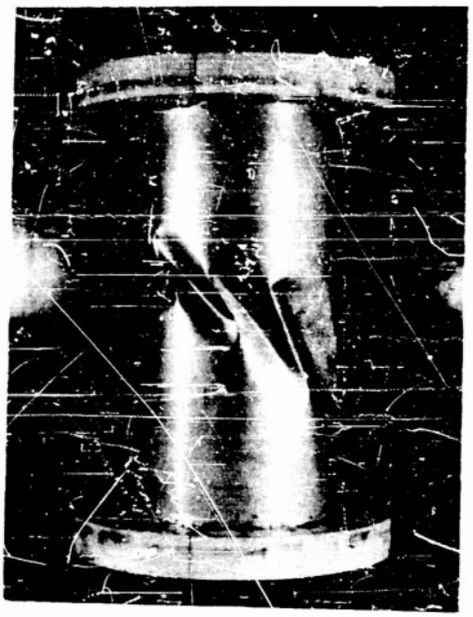

FIG. 19
12" CCA

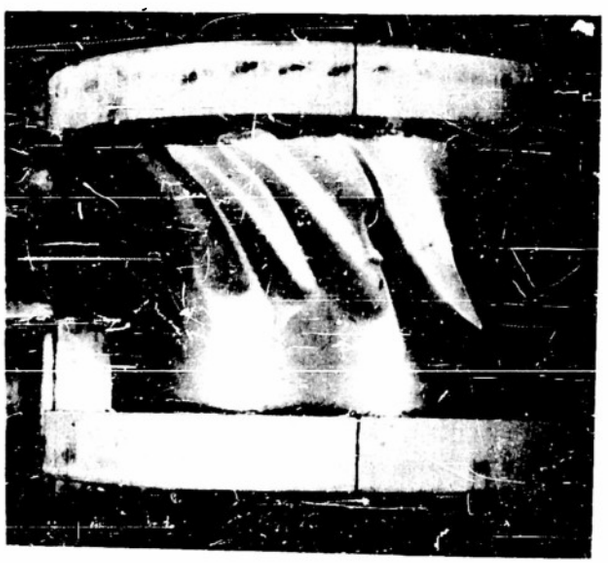

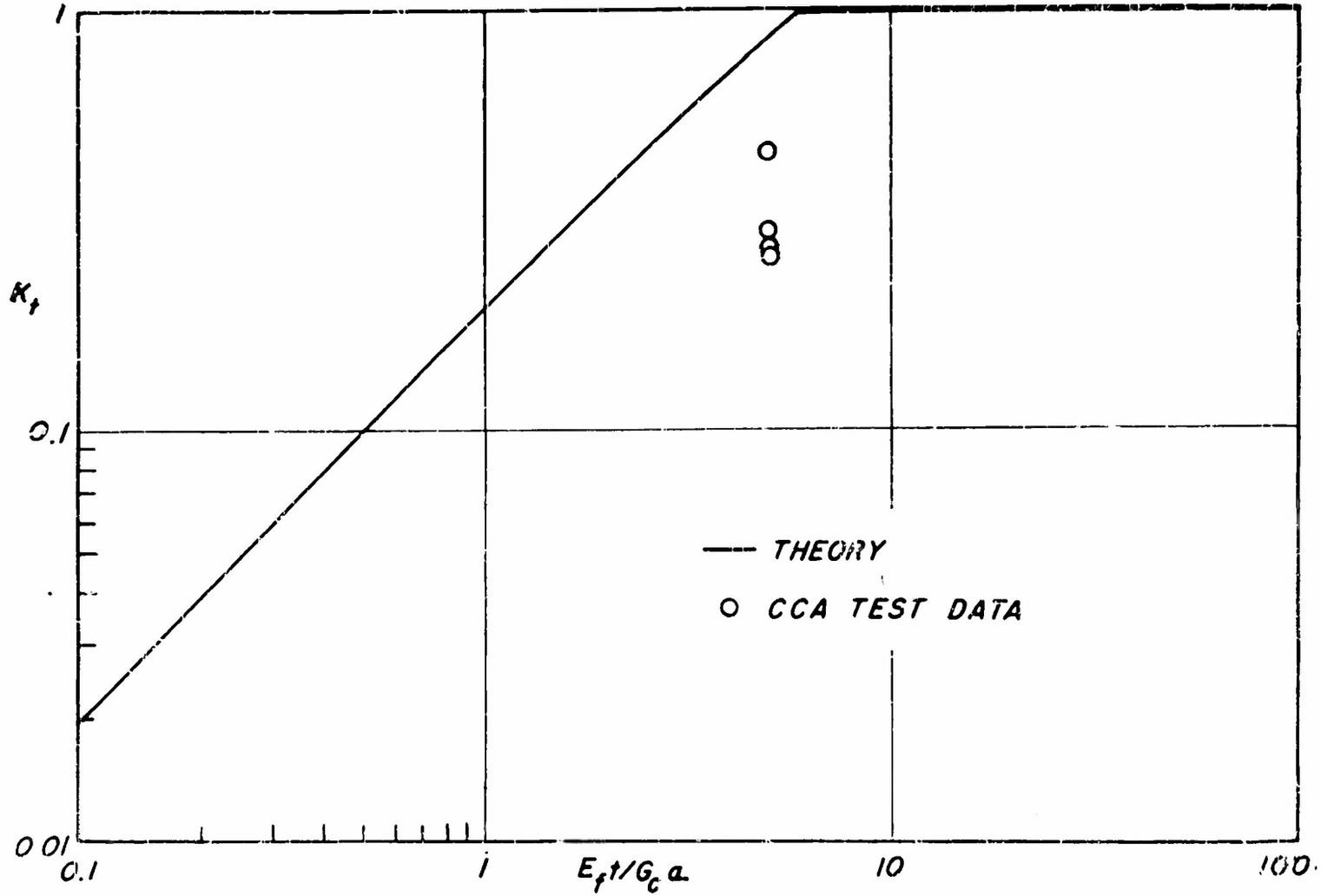

FIGURE 20. THEORETICAL AND EXPERIMENTAL BUCKLING COEFFICIENTS FOR $a/(h+t) = 48$

FIGURE 21. CORRELATION OF THEORY AND EXPERIMENT FOR EGB CYLINDERS

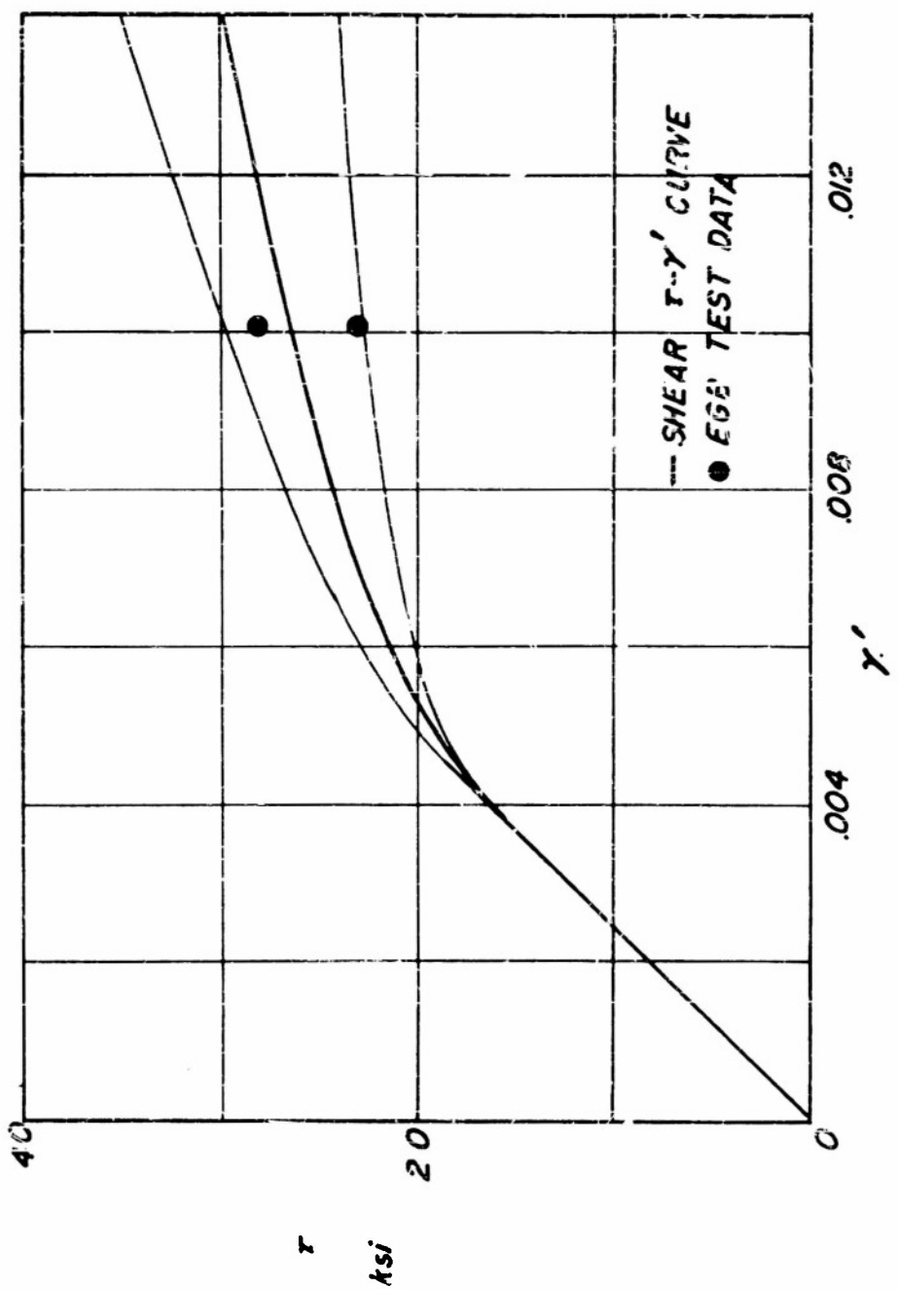

FIGURE 22

BENDING TEST SET-UP

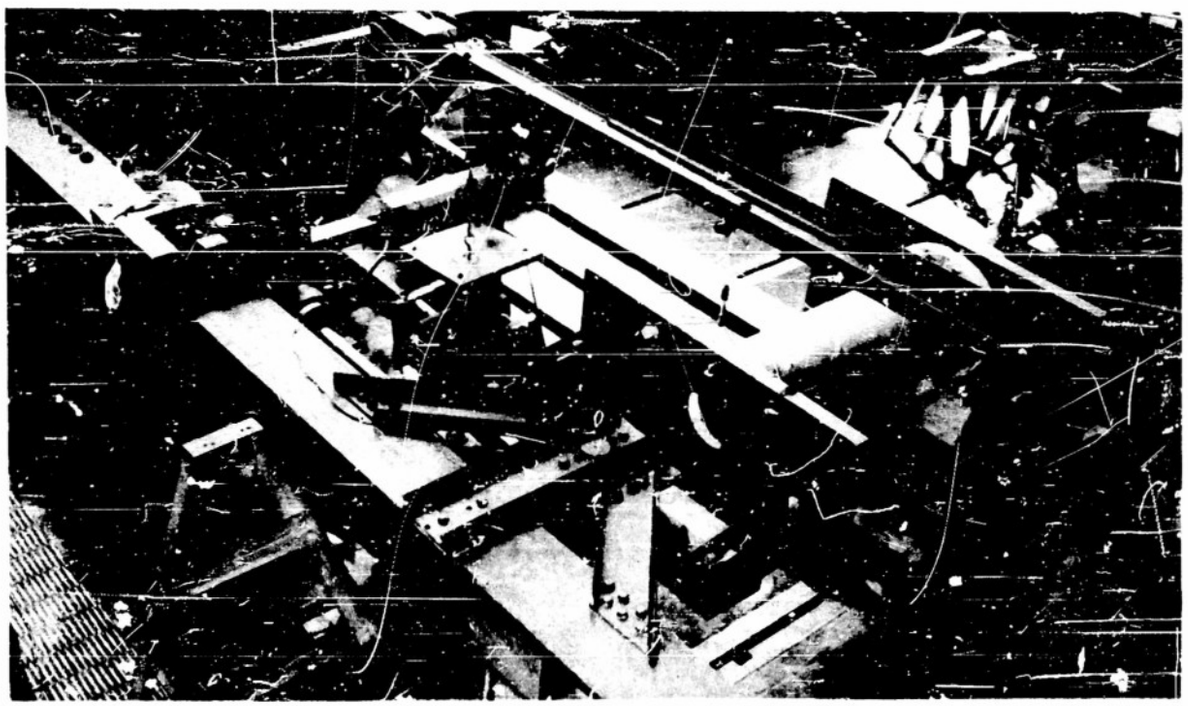

FIGURE 23. COMPRESSIVE STRESS STRAIN CHARACTERISTICS OF FACES 0.010" 24S-T WITH GRAIN

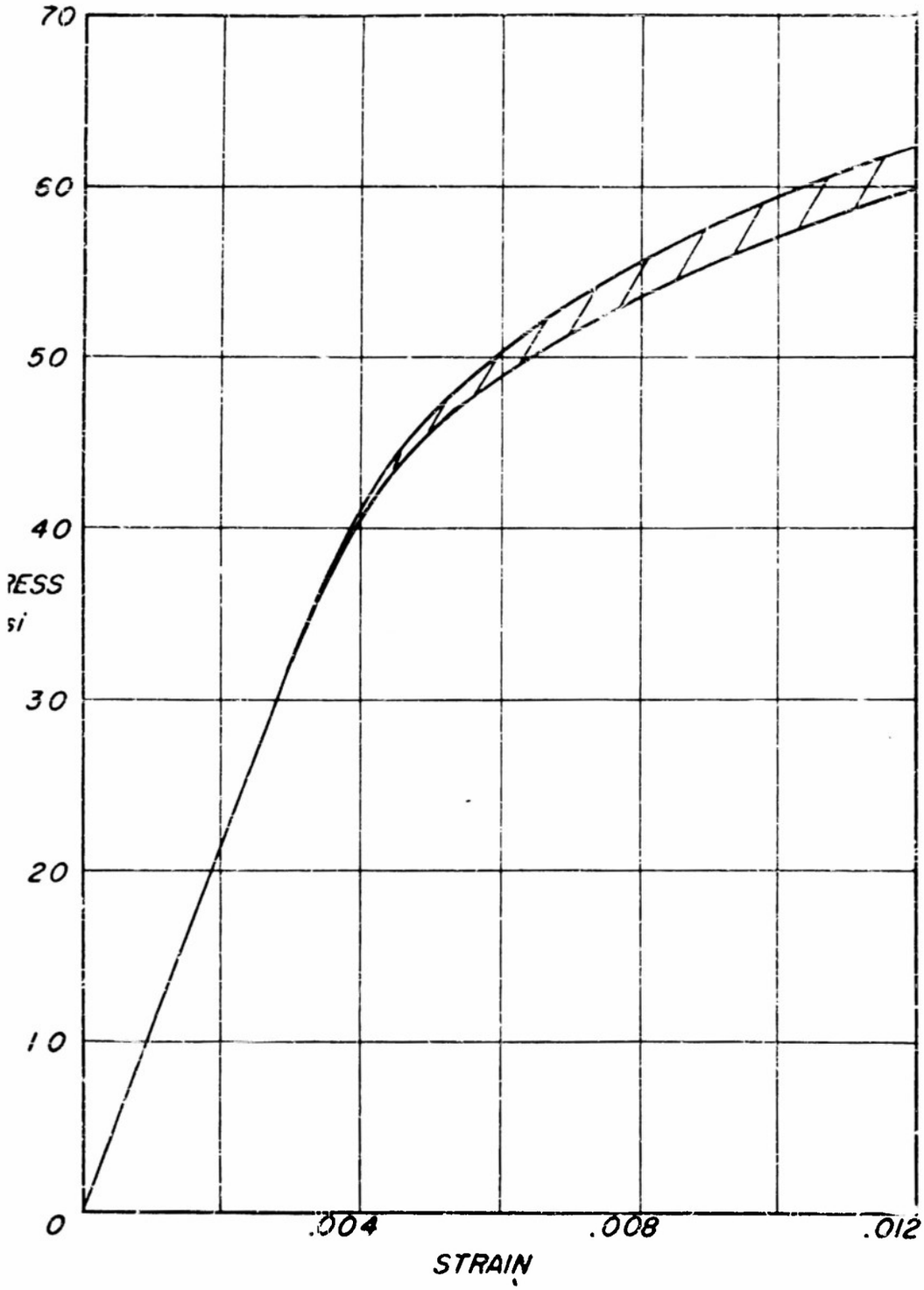

FIGURE 24

OVERALL BENDING BUCKLING
OF 1/8" CYLINDERS